

Manuscript Number: JFUE-D-16-00119R1

Title: Flash boiling in a multihole G-DI injector - Effects of the fuel distillation curve

Article Type: Research paper

Keywords: flash boiling; direct injection spark ignition; spray angle; gasoline; distillation curve

Corresponding Author: Dr. Roberto Donde', Ph.D

Corresponding Author's Institution: CNR-ICMATE

First Author: Lucio Araneo, PhD

Order of Authors: Lucio Araneo, PhD; Roberto Donde', Ph.D

Abstract: The effects of fuel temperature and chamber pressure on the spray of a multi-hole G-DI injector were analyzed in a quiescent test chamber. The analysis was focused on the behavior of the global spray angles both close and far from the injector. Three pure hydrocarbons (n-hexane, n-heptane, and isooctane), three gasolines of known distillation curve and a commercial 95 RON gasoline from a gas station were utilized. The tests were performed at four chamber pressures (atmospheric, 80kPa, 60 kPa and 40 kPa) and the fuel temperature was varied from 30°C to 110°C.

The results for n-hexane and gasolines were very similar, while n-heptane and isooctane showed a different behavior. The ratio between the fuel saturation pressure at the operating temperature and the air pressure (ps/pa) is confirmed as a fundamental parameter for spray angle data reduction. The near field spray angle data for pure hydrocarbon fuels merge to a unique curve when plotted in function of ps/pa. An approximated method to deduce the gasoline saturation pressure curves starting from the distillation curve is presented. Using the calculated saturation pressures for the reduction of near field spray angle data for the gasolines, a unique curve is obtained, coincident with that of the tested pure hydrocarbons. In alternative, from the results obtained for a fuel of known saturation pressure curve, it is possible to obtain a direct correlation between near field spray angle and saturation pressure. From this relationship, an approximated saturation pressure curve from the experimental angle measurements obtained on the same injector for an unknown fuel can be derived.

1 **Flash boiling in a multihole G-DI injector – Effects of the fuel distillation curve.**

2

3 Lucio ARANEO^{a,b}, Roberto DONDE^{a*}

4 a CNR-ICMATE, via Cozzi 53, 20125 Milano, Italy

5 b Politecnico di Milano, Dipartimento di Energia, via Lambruschini 4A, 20156 Milano, Italy

6 * Corresponding author, roberto.donde@cnr.it

7 ***Abstract***

8 The effects of fuel temperature and chamber pressure on the spray of a multi-hole G-DI injector
9 were analyzed in a quiescent test chamber. The analysis was focused on the behavior of the global
10 spray angles both close and far from the injector. Three pure hydrocarbons (n-hexane, n-heptane,
11 and isooctane), three gasolines of known distillation curve and a commercial 95 RON gasoline from
12 a gas station were utilized. The tests were performed at four chamber pressures (atmospheric,
13 80kPa, 60 kPa and 40 kPa) and the fuel temperature was varied from 30°C to 110°C.

14 The results for n-hexane and gasolines were very similar, while n-heptane and isooctane showed a
15 different behavior. The ratio between the fuel saturation pressure at the operating temperature and
16 the air pressure (p_s/p_a) is confirmed as a fundamental parameter for spray angle data reduction. The
17 near field spray angle data for pure hydrocarbon fuels merge to a unique curve when plotted in
18 function of p_s/p_a . An approximated method to deduce the gasoline saturation pressure curves
19 starting from the distillation curve is presented. Using the calculated saturation pressures for the
20 reduction of near field spray angle data for the gasolines, a unique curve is obtained, coincident
21 with that of the tested pure hydrocarbons. In alternative, from the results obtained for a fuel of
22 known saturation pressure curve, it is possible to obtain a direct correlation between near field spray
23 angle and saturation pressure. From this relationship, an approximated saturation pressure curve

24 from the experimental angle measurements obtained on the same injector for an unknown fuel can
25 be derived.

26 **Highlights**

- 27 ▪ The saturation pressure curve can be obtained from the fuel distillation curve.
- 28 ▪ The saturation pressure curve can be obtained from the experimental spray angle.

29

30 **Keywords:** flash boiling; direct injection spark ignition; spray angle; gasoline; distillation curve

31 **Nomenclature**

32 c_p specific heat

33 p_a air pressure

34 p_s saturation pressure

35 T_f fuel temperature

36 T_s saturation temperature

37 ΔH_v latent heat of evaporation

38 ρ_l liquid density

39 ρ_v vapor density

40 **Abbreviations**

41 **ASOI** After Start Of Injection

42 **ASTM** American Society for Testing and Materials

43 **DIPPR** Design Institute for Physical Properties

44 **G-DI** Gasoline Direct Injection

45 **NIST** National Institute of Standards and Technology

46 **RON** Research Octane Number

47 **SAE** Society of Automotive Engineers

48 **TBP** True Boiling Point

49 *1. Introduction*

50 It is well known that rapid evaporation occurs when a liquid is injected in an ambient at pressure
51 below its saturation pressure. The sensible heat of the fuel provides the latent vaporization heat for a
52 fraction of the liquid mass. After the pioneering work by Brown and York [1], numerous studies on
53 the phenomenon in pools, ducts, jets, films and sprays were published. Although the physical bases
54 are the same, the practical effects of interest in the various configurations could be different. Many
55 studies were focused on transition from Rayleigh jet regime to spray regime by flash boiling. The
56 aim was to obtain a good atomization with low pressure atomizers. An overview of the state of the
57 art on this aspect of flash boiling is given in Sher et al. [2]. Different is the scope of the present
58 work. In this case the effects of the phenomenon on a real G-DI injector at real injection pressure
59 are studied. It means that a fully developed breakup regime is considered even in absence of flash
60 boiling.

61 As the G-DI technology developed, the behavior of different injector types was reported in
62 literature. From the first studies devoted to swirl injectors [3-9], the attention lately moved to other
63 injector types [10-24], however the studies on swirl injectors were not abandoned [25]. From the
64 experimental results reported in the cited literature, a clear effect of flash boiling both on the spray
65 shape and on the droplet diameters was noticed both for swirl and for multi-hole atomizers. The
66 effects on both types of atomizers are similar. In particular, flash boiling causes an increase of the
67 spray angle at the nozzle exit [4, 5, 9, 10, 12, 13, 16, 19, 24], that is followed by a contraction of the
68 angle as the distance from the nozzle increases [5, 10, 12-14, 18].

69 It is evident that the choice of the position where the spray angle is measured strongly affects the
70 results, so quantitative comparison of works from different origins with different processing criteria
71 cannot be immediately performed. In some cases, the angle definition gives as a consequence a
72 behavior apparently opposite to the actual one. It would be desirable to define some standard
73 procedures to measure the spray angles in order to obtain a comparable description of the actual
74 spray behavior.

75 The SAE J2715 [26] Recommended Practice has some limitations when applied to a flashing spray.
76 Depending on the injector design, the recommended measurement range from 5mm to 15mm could
77 interest a region where the transition between angle increase and angle decrease occurs.
78 The spray penetration is affected both by the degree of overheating and by the ambient pressure [12,
79 19, 21, 24]. The mean droplet size was observed to decrease in presence of flash boiling [4, 6, 11,
80 14, 16, 21]. These effects could be either favorable or detrimental depending on the applications,
81 from this fact follows the importance of the studies about this topic. For this reason the authors
82 carried up in the past studies on a G-DI swirl injector using simple fuels [9]. The results, reported in
83 Figure 1, demonstrated that the angle at the exit of the injector was greatly influenced by flash
84 boiling. Infact as soon as the phenomenon starts to occur the spray angle increases. Testing
85 mixtures of n-pentane and isooctane in different percentage at atmospheric pressure, the angle
86 increase starts to occur at higher temperature as the percentage of the higher boiling component
87 (isooctane) is increased (Figure 1a). Plotting the same results in terms of the ratio between
88 saturation pressure and ambient pressure (p_s/p_a) instead of temperature, the experimental curves
89 merge in a unique curve as shown in Figure 1b. When the value of p_s/p_a becomes greater than one
90 the spray angle starts to increase and for values greater than 1.5 the data can be fitted by a
91 logarithmic curve. Furthermore, the saturation pressure to be considered resulted to be the average
92 saturation pressure of the mix, with no dominant effects of the lighter element. Considering these
93 previous results, the authors decided to extend the investigation to a new generation multi-hole
94 injector and different distillation gasolines. The examined results regard mainly the effects of flash
95 boiling on the near field global angle of the injector spray. The main scope of the work is the setup
96 of a procedure to study the effect of different distillation curve gasolines on the behavior of the
97 injector spray in flash boiling conditions.

98 2. *Experimental setup and procedure*

99 A six holes G-DI injector was tested in a constant volume chamber. The spatial distribution of the
100 injector jets at 30 mm distance from the tip is reported in Figure 2, where the arrow indicates the
101 line of sight of the camera. Four of the six jets are nearly aligned in the visualized image plane,
102 while the other two are aligned along the line of sight

103 The nominal value of the spray angle in the image plane is 72° and the nominal single beam angle is
104 19° . The nominal static mass flow rate is 923.5 grams n-heptane per minute at 10 MPa injection
105 pressure.

106 The test chamber has an internal volume of 10 liters (206 mm internal diameter and 300 mm height)
107 and has four 90 mm diameter windows positioned at 0° , 110° , 180° and 270° angles for
108 visualizations and optical diagnostics. The chamber walls can be heated by electric cartridges and
109 the input air can be preheated in an electrically heated reservoir. The air temperature inside the
110 chamber is monitored by means of a J type thermocouple whose tip is placed near the injector tip
111 but out of the spray range. In the present study, the chamber air temperature was kept at 25°C .

112 For the tests, the chamber pressure was varied from ambient pressure down to 40 kPa absolute
113 pressure using a compressed air ejector. The pressure regulation was obtained acting both on ejector
114 applied air pressure and on input airflow. The airflow was optimized to have a complete evacuation
115 of the injected fuel during the interval between two consecutive injections without influencing the
116 spray behavior. Moreover, the airflow was effective in avoiding the increase of the chamber air
117 temperature due to the presence of the injector heater.

118 The fuel was pressurized using a sac pressure accumulator in order to avoid direct contact of the
119 fuel with the pressurizing gas. The fuel was pumped in the circuit by a normal automotive electric
120 pump and, after a period of recirculation in order to purge the circuit from gas bubbles, the gas
121 pressure in the accumulator was reduced below the pump pressure to allow the accumulator filling.
122 After that, the filling circuit was closed and the fuel was pressurized to the wanted injection
123 pressure by supplying nitrogen to the gas section of the accumulator. The pressure was controlled

124 by a pressure transducer and a feedback circuit acting on a solenoid valve. The tests were performed
125 at 10 ± 0.05 MPa fuel injection pressure.

126 The injector was placed at the center of the upper flange of the chamber using an appositely
127 designed adapter. The injector was surrounded by an oil jacket heated by two electric cartridges
128 placed on the sides. A J-type thermocouple placed in contact with the injector measured the tip
129 temperature and gave the feedback to the electric cartridges PID controller.

130 The injector nose temperature was varied from 30 to 110°C with 20°C steps. The injection duration
131 was set to 3ms and the repetition rate was limited to 0.5 Hz in order to guarantee that the fuel
132 temperature was as close as possible to that of the injector nose. The low injection frequency also
133 facilitated the test chamber air renewal between the injections. The steadiness of the injection
134 temperature was controlled a posteriori by observing the absence of any particular temporal trend in
135 the results obtained at constant conditions.

136 Seven different fuels were investigated: three gasoline formulations of known distillation curve, a
137 commercial gasoline (RON 95) from a gas station, n-hexane, n-heptane and isooctane.

138 The effects of flash boiling on the spray structure were studied by comparing the images of the
139 spray in different operative conditions.

140 The imaging setup consisted in a Z-schlieren apparatus [27] without knife, thus allowing backlight
141 imaging and no perspective effects. A stroboscopic flash lamp with a flash duration of about 30 μ s
142 was used as light source and the images were taken by a PCO Sensicam camera setting the exposure
143 time at 3 μ s. The timings of injector, flash lamp and CCD camera were controlled by a multichannel
144 pulse generator. Particular care was taken in the optical system alignment in order to have a uniform
145 background and a neat contrast with the spray edge. The background quality was used also as a
146 criterion for the airflow setting. The airflow was increased and the repetition rate reduced until the
147 presence of residual fuel fog from the previous injection was negligible. The optical setup was
148 adjusted to have an image spatial resolution of 0.1 mm per pixel. This choice was dictated by the
149 compromise between the necessity of a complete view of the spray far field and the accuracy in

150 near field angle measurement. As a result, the pixel resolution introduces an uncertainty in the near
151 field angle measurement of about 3° on the spray angle at cold conditions, This uncertainty
152 decreases to 1.5° at 60° spray semiangle, 0.6° at 70° and 0.15° at 80° spray semiangle. This
153 uncertainty was found to be within the shot to shot experimental variability.

154 Series of thirty single shot images at 1, 2 and 3 ms delay ASOI were taken for every experimental
155 condition. Every single image was analyzed to extract the angle data. The results were then
156 averaged and the standard deviation value was calculated.

157 The global envelope of the spray was considered for the measurement of the spray angles, therefore
158 the angles between the external edges of jet 2 and jet 6 of the spray were measured. In particular,
159 the spray near field angle (from 0 to 1mm from the nozzle) and far field angles (in the ranges 20-
160 30mm, 30-40mm and 40-50mm from the nozzle) were measured.

161 The images were automatically analyzed using an “ad hoc” macro running in Image Pro Plus
162 software. The first step of the image analysis consisted in a normalization, based on the intensity
163 value of a region of the image far from the spray, to correct for possible shot-to-shot variation of the
164 light intensity. Then a background subtraction using an image taken before the injector opening was
165 performed. The following steps of the analysis for the near field angle measurement are reported in
166 Figure 3. The resultant image (a), where the spray appears dark on a bright background, was
167 inverted to have a white spray on a dark background (b). Due to the good contrast given to the
168 images by the optical setup, a sharp transition between the spray image and the background was
169 obtained. After a preliminary sensitivity analysis a threshold of 10% of the range of the intensity
170 profile was chosen to identify the spray edge. The image was then binarized using this threshold (c).
171 The angles were calculated by connecting the points determined by the intersections of the spray
172 profile with two lines normal to the spray axis traced at the beginning and at the end of the defined
173 distance range (d). It is particularly important to choose a very short distance for the near field
174 angle. This because the dominance of the flash boiling phenomenon in enlarging the spray contour
175 is very short living. At few millimeters from the nozzle the spray profile begins to bend toward the

176 spray axis due to the induced air flow field. An example is shown in Figure 4 where a binarized
177 image of a highly flashing spray is reported. The reference lines traced at a distance of 1mm and
178 5mm from the injector tip allow to appreciate at a glance how close to the nozzle the induced air
179 flow field begins to dominate the spray shape. This image shows also a limitation in the adopted
180 method as, in these conditions, even in the distance range of 1mm from the injector tip, the spray
181 edge is not linear. For this reason at 1 mm distance from the nozzle a near field spray angle value
182 lower than the real angle at the nozzle exit is obtained.

183 A resume of the experimental conditions is given in Table 1

184 **3. *Experimental results***

185 As reported before, the aim of this work was the study of the effects of flash boiling on the spray
186 structure of different fuels. This was obtained by increasing the fuel temperature, at constant air
187 pressure, from 30 °C up to 110 °C and measuring some spray characteristic angles. The procedure
188 was repeated at four different air pressure values (40, 60, 80 kPa and atmospheric pressure) for each
189 one of the seven fuels.

190 In Figure 5, two images of the spray both in absence (a) and in presence (b) of flash boiling are
191 compared. Close to the nozzle, the spray angle increases for the effect of flash boiling. After the
192 initial angle widening, the spray side boundary tends to curve toward the axis causing a contraction
193 of the spray width. This spray collapse was observed by many researchers [5, 10, 12-14, 16, 18, 21,
194 25] both in swirled and in multi-hole injectors. It was explained by the decrease of droplet mean
195 diameter observed when flashing occurs [21, 25]. In fact, smaller droplets are more easily driven
196 toward the spray axis by the induced airflow.

197 In Figure 6a-d, the average values of the spray semiangle measured at 1 mm distance from the
198 nozzle are reported in function of the fuel temperature for each test chamber pressure value. The
199 error bars shown both in these and in all the following graphs indicate plus-minus one experimental
200 standard deviation around the mean. A clear difference in the behavior of isooctane and n-heptane

201 with respect to the other fuels is noticed. For these pure hydrocarbons, at atmospheric pressure (Fig.
202 6a), the spray angle increase occurs around 100°C. This is in agreement with their atmospheric
203 boiling points of 99°C and 97°C. The n-hexane curve indicates that the angle increase occurs at
204 about 70°C. Even for this fuel the transition temperature is close to the boiling point, that, for n-
205 hexane, is 67°C. The fact that all the tested gasolines have a behavior very close to that of n-hexane
206 would indicate that their saturation temperature at ambient pressure is similar. Moreover, it is clear
207 that in these operating conditions, flash boiling start to affect the spray structure even at low
208 superheating.

209 A similar behavior is noticed in the whole range of the experimental chamber air pressures
210 explored. When the air pressure is changed, the curve of the near field spray angle bends up at
211 temperature values decreasing with pressure decrease. For all the pressure values, all the gasolines
212 and n-hexane show a similar behavior, while n-heptane and isooctane can be clearly distinguished
213 from the other fuels. This difference was already observed and emphasized by other researchers [14,
214 16, 22], coming to the conclusion that the use of these hydrocarbons as test fluids in flash boiling
215 experiments could lead to wrong indications.

216 In Figure 7(a-d) the behavior of the far field spray angle in the range 20-30 mm distance from the
217 nozzle is shown. High angle variations are indicated by the large error bars, however a clear
218 reduction of the angle when the fuel temperature is increased is shown. Therefore, the measurement
219 at different distances from the injector tip can give opposite results in terms of spray angle.

220 The knowledge of the saturation pressure curve of the pure hydrocarbons (n-hexane, n-heptane and
221 isooctane), gives an immediate clear view of the link existing between the boiling point at the test
222 air pressure and the flash boiling effects on the spray structure. In fact, as soon as the fuel
223 temperature reaches the boiling value corresponding to the air pressure in the test chamber, an
224 immediate increase of the near field angle of the spray is noticed.

225 Different characteristic parameters were presented in literature to correlate the behavior of some of
226 the spray characteristics in presence of flash boiling. Typically the superheating degree ($T_f - T_s$), the

227 Jakob number in its form $Ja=(\rho_l/\rho_v)c_p(T_f-T_s)/\Delta H_v$ and the ratio between the saturation pressure and
228 the ambient pressure were used for this scope. This last parameter was presented in literature under
229 different forms: as $\Pi=(p_s-p_a)/p_a$ [4], (p_s/p_a) [9] and (p_a/p_s) [12]. The authors want to underline that
230 the use of these parameters is limited to injectors that in normal conditions work in fully developed
231 breakup regime. As observed by Lamanna et al. [28], in different working conditions these
232 parameters are not controlling the onset of flashing regime.

233 As already reported in a previous work [9], plotting the near field spray angle in terms of the ratio
234 between the saturation pressure at the experimental temperature and the air pressure (p_s/p_a) , all the
235 curves tend to merge.

236 An example is reported in Figure 8, where the data obtained for n-hexane are reported both in terms
237 of fuel temperature (a) and in terms of (p_s/p_a) (b)

238 Looking at Figure 8b an effect of ambient pressure is noticed. As ambient pressure decreases the
239 spray angle curve become slightly steeper, however, for the current purpose, this effect can be
240 considered negligible.

241 In the present data analysis all the three parameters cited above will be employed and compared for
242 the analysis of the three pure hydrocarbons tested. As it will be shown, all the three parameters
243 permit a good data correlation, merging the curves obtained at different chamber pressures and
244 different fuels in a unique approximated fitting curve. The dispersion of the subcooled angle data
245 makes difficult a precise determination of the beginning of the ascending branch of the curves for
246 the fuels. So a clear comparison of the different fuels in this respect is critical. For the same reason
247 the fitting data range was chosen considering only the data that, from the graphs, clearly appeared
248 as pertaining to the rising part of the curve. The same data range was used for the global fittings
249 shown in the following figures.

250 In Figure 9 the near field semiangle of all the pure hydrocarbon fuels employed is reported in terms
251 of superheating degree (T_f-T_s) . The angle starts to increase when $(T_f-T_s) \approx 0$. The data were fitted
252 for $(T_f-T_s) > 5^\circ\text{C}$ and the best data fitting is a linear function with $R^2 = 0.89$.

253 In Figure 10 the same data are reported in terms of Jakob number. In this case the data were fitted
254 for $Ja > 10$. The best fitting function is logarithmic and its R^2 is 0.95

255 In Figure 11 the correlating parameter is the p_s/p_a ratio. The data were fitted for $p_s/p_a > 1.2$. The best
256 fitting function is logarithmic and its R^2 is 0.93

257 All the three correlation parameters are suitable for data reduction. The fitting in terms of p_s/p_a ratio
258 has an R^2 only slightly lower of that obtained with Jakob number. However the parameter p_s/p_a has
259 the advantage of being easier to calculate and it is more physically sound that flash boiling starts to
260 occur at $p_s/p_a \geq 1$. For these reasons and for what will be shown later, the p_s/p_a ratio was chosen for
261 the following analysis. It is clear from the figure that the slope for n-heptane is higher than that of
262 the other two fuels. In particular the individual slope values are: 19.5 for n-heptane, 17.7 for
263 isooctane and 17.9 for n-hexane. On the other hand, the average subcooled angle for isooctane is
264 higher than that of n-heptane. However, the $\pm 5\%$ bands of the global fitting curve reported in the
265 plot show a good degree of approximation for this way of comparing the data collected in different
266 operating conditions.

267 As it was shown in the previous figures, the onset of flash boiling causes an increase of the near
268 field spray angle. The opposite effect is shown in Figure 12 for the far field angle. In this case,
269 when $p_s/p_a > 1$ the angle shows a clear decrease. Thus, the expansion of the near field spray angle
270 due to flash boiling has the consequence of contracting the far field spray angle up to the spray
271 collapse. As previously mentioned, this effect is commonly explained by the decrease of the droplet
272 mean diameter, however some other factors influencing the overall induced air flow field could be
273 accounted for. For example, Moon at al. [25] observed clear dissimilar effects between flashing and
274 non flashing conditions, in terms of pressure difference between inner and outer part of the spray of
275 a swirl injector. Even more complex is the case of multihole injectors, where the different spray
276 plumes interact in different ways depending on the injector pattern. It is also to be noticed that the
277 subcooled angle measured in the far field is considerably smaller than that measured in the near

278 field. Obviously, even in subcooled conditions the induced air flow field has the effect of curving
279 the spray side edge toward the axis as the distance from the nozzle increases.

280 As shown in Figure 6 and 7 the tested gasolines have a behavior similar to that of n-hexane. It is
281 conceivable that the saturation pressure curves of the gasolines are close to that of n-hexane and that
282 both the increase of the near field angle and the decrease of the far field angle for the gasolines start
283 at $p_s/p_a=1$. In the following section an approximated method for the calculation of the saturation
284 pressure curve for a gasoline starting from its distillation curve and its aromatic content will be
285 described.

286 ***4. Construction of the saturation pressure curve from the ASTM D86*** 287 ***distillation curve.***

288 The data available for the different types of gasoline used in the tests are:

- 289 • the ASTM D86 distillation curve
- 290 • the aromatic content

291 The distillation curves of the three gasolines used in these tests are presented in Figure 13.

292 The volumetric aromatic contents were 30.9% for Fuel04, 34.2% for Fuel06 and 29.2% for Fuel08.

293 From these data, it was possible to obtain an approximated saturation pressure curve.

294 The first step was the transformation of the ASTM D86 curve of the gasoline in the corresponding
295 True Boiling Point (TBP) curve. This passage was obtained through the analytical correlation given
296 by Riazi [29]

$$297 \quad \text{TBP}=a (\text{ASTM D86})^b \quad (1)$$

298 where the ASTM D86 temperatures are in Kelvin and the constants a and b, at different values of
299 the volume percentage of the distillation curve, are given by Riazi [29].

300 In Figure 14, the given ASTM D86 distillation curve and the True Boiling Point calculated curve
301 for one of the gasolines are reported.

302 From the volume distillation intervals of the TBP curve seven “pseudocomponents” were defined.
303 These pseudocomponents are characterized by the average boiling temperature of the distillation
304 interval and their composition is approximated by a mixture of paraffinic and aromatic
305 hydrocarbons. As the lower boiling aromatic is benzene (80°C), the pseudocomponents
306 characterized by a lower boiling temperature were considered as composed by paraffines. The other
307 pseudocomponent composition was approximated by a mixture of paraffines and aromatics in a
308 constant proportion to respect the given total aromatic content.

309 Olsen [30] gives regression curves, calculated from DIPPR data, for molar density in function of the
310 boiling temperature for n-paraffins, isoparaffins, cycloalkanes and mono-aromatics. The curves of
311 paraffins and isoparaffins are almost coincident and the curve of cycloalkanes is approximately an
312 average of the curves of n-paraffins and monoaromatics.

313 The molar volume fraction x_i of each pseudocomponent was then obtained from the average molar
314 density of its paraffinic and aromatic content obtained from Olsen's curves.

315 Each pseudocomponent saturation pressure p_{si} was then estimated using the model presented by
316 Dutt [31] for pure hydrocarbons.

317 An Antoine type relationship between vapor pressure and temperature is given:

$$318 \quad \log(p_{si}) = A - B/(C+T) \quad (2)$$

319 The constants B and C are given in terms of boiling temperature T_b as:

$$320 \quad B = m + nT_b \quad (3)$$

$$321 \quad C = m' + n'T_b \quad (4)$$

322 the constants A, m, n, m', n' are given by Dutt [31] for the different families of hydrocarbons.

323 The p_{si} value was obtained, in the same way of the molar fraction, by averaging the values of
324 saturation pressure obtained for paraffines and aromatics, according to the given content in the
325 gasoline. The global saturation pressure curve was obtained from the sum over the seven
326 pseudocomponents:

$$327 \quad p_s(T) = \sum x_i p_{si}(T). \quad (5)$$

328 The saturation curves obtained with this method are reported together with isooctane, n-heptane and
329 n-hexane curves in Figure 15.

330 These saturation pressure curves, calculated for the three gasolines whose distillation curve was
331 known, permit to plot the near field spray angles in the same way as for the pure hydrocarbons. This
332 is shown in Figure 16, where the dashed lines reported are the same of Figure 9. This means that
333 even in this approximated approach the near field angle expansion starts when the (p_s/p_a) ratio is
334 about equal to one.

335 ***5. Construction of the saturation pressure curve from experimental near field***
336 ***angle.***

337 For Fuel95, whose distillation curve is unknown, it was not possible to apply the same method of
338 data reduction. However, considering valid the behavior observed for the other fuels, it is possible
339 to found, from the experimental data concerning the near field angle variation with fuel temperature
340 (Figure 17), an approximate saturation curve for this gasoline. Considering the relationship linking
341 the spray angle to p_s/p_a for n-hexane valid also for the other fuels, the value of p_s/p_a for Fuel95 can
342 be obtained from the experimental spray angles. In this case the influence of ambient pressure, that
343 was considered negligible for data reduction, is accounted for. Therefore, using the logarithmic
344 fittings of the hexane spray angle data with $p_s/p_a > 1$ at different ambient pressures, it was possible
345 to obtain the p_s/p_a value from the Fuel95 spray angle data obtained at the same air pressure. In
346 Figure 18 the saturation pressure values deduced from the experimental spray angles of Fuel95 at
347 different air pressure are reported in terms of absolute fuel temperature. These data were fitted
348 obtaining a curve of the type $p_s = \exp(a - b \cdot 1/T)$. As shown in Figure 15, the saturation pressure curve
349 of Fuel95 obtained with this procedure falls among the other gasoline curves. As the real saturation
350 pressure curve for this gasoline is not available, a direct evaluation of the accuracy of the method
351 for this gasoline is impossible. For this reason, the same procedure was applied to a fuel of known
352 saturation pressure curve. In particular the method was applied to n-heptane data. The obtained

353 curve is reported in Figure 15 and it results to be very close to the one given by NIST [32]. The
354 difference between the real and the reconstructed saturation pressure varies, in the range of interest,
355 from 6% to 3%.

356 It is obvious that plotting the Fuel95 results in terms of p_s/p_a using the found $p_s(T)$ curve, the data
357 merge on the same curve of the other fuels.

358 **6. Conclusions**

359 The experimental results of this study show the effects of the increase of fuel temperature on the
360 spray angles of a multi-hole injector operated with three pure hydrocarbons (n-hexane, n-heptane,
361 and isooctane), three gasolines of known distillation curve and a commercial 95 RON gasoline. The
362 results are mainly focused on the near field angle, measured in the range of 1mm from the injector
363 tip. For comparison, a far field angle, measured in the range between 20 and 30 millimeters from
364 the injector tip, was also reported.

365 A first analysis was performed on the experimental results obtained with pure hydrocarbons to have
366 a reliable data set for a comparison with literature results and with the following analysis based on
367 the results obtained with the different gasolines. Although it is impossible to compare quantitatively
368 the results reported in literature because of the absence of a common procedure for the spray angle
369 measurement under flash boiling conditions, some general trends were confirmed. In particular: the
370 spray angle data obtained at different fuel temperature and different chamber air pressure can be
371 compared in terms of the ratio between saturation pressure at the given fuel temperature and
372 chamber pressure (p_s/p_a). In this way the curves for the different hydrocarbons at different chamber
373 pressures tend to merge to a unique curve.

374 To compare in the same way the results obtained for the gasolines, an approximate saturation
375 pressure curve was calculated. Two procedures were presented.

- 376 1. Starting from the ASTM D86 distillation curves, it was possible, using correlations reported
377 in literature, to find an approximated saturation curve for each gasoline. From these curves

378 it was possible to plot the gasoline spray angles in terms of p_s/p_a ratio. In this type of plot
379 the gasoline data have the same behavior of the pure hydrocarbon data.

380 2. As the near field spray angle for a given injector is correlated with p_s/p_a ratio, it is possible
381 to obtain an approximated saturation curve $p_s(T)$ for an unknown composition fuel by
382 comparing its near field spray angle behavior on the same injector with that of a fuel of
383 known $p_s(T)$ curve.

384 Finally, from the brief literature survey reported in the introduction and the above experimental
385 outcomes, a general conclusion can be draft: a suitable recommended practice for the testing of G-
386 DI fuel injectors in flash boiling conditions is needed.

387 The spray angle, in flash boiling conditions, has a transition from expanding in the near field to
388 contracting in the far field. Therefore, the most urgent point is a spray angle definition that could
389 give, with a good approximation, an "initial" spray angle avoiding the following transition region.
390 In this way some ambiguous results reported in literature will be avoided. Moreover, as the
391 maximum effect of flash boiling occurs at the nozzle exit, this angle definition will give the
392 maximum sensitivity of the measured angle to the increase of p_s/p_a ratio.

393 The second point is the choice of n-hexane as reference fuel. This choice seems to be generally
394 accepted in laboratories where flash boiling is a consolidated research interest, however in other
395 laboratories either the standard n-heptane indicated by the SAE J2715 procedure or isooctane are
396 commonly utilized. Clearly, any pure hydrocarbon can be used as far as the data are normalized
397 with the p_s/p_a ratio. However, since n-hexane and gasoline have a similar behavior with respect to
398 flash boiling, the choice of n-hexane as reference fuel will simplify testing procedures.

399 The attempt to obtain an injector independent description of the flash boiling spray in its whole
400 aspect, based on simple correlations and normalizations is quite ambitious. Nevertheless, a common
401 experimental background could facilitate the direct quantitative comparison of the experimental
402 data from different laboratories supplying a vast and reliable database for model validation.

403

404 References

- 405 [1] Brown R. and York J.L. Sprays formed by flashing liquid jets, *AIChE Journal* 8(2) ,
406 149–153, (1962)
- 407 [2] Sher E., Bar-Kohany T. and Rashkovan A., Flash-boiling atomization, *Progress in*
408 *Energy and Combustion Science* 34, 417–439 (2008)
- 409 [3] Vanderwege, B. A., and Hochgreb S. The effect of fuel volatility on sprays from high-
410 pressure swirl injectors. *Symposium (International) on Combustion*, 27(2). 1865-1871,
411 Elsevier, (1998).
- 412 [4] Vanderwege, Brad Alan. The effects of fuel volatility and operating conditions on
413 sprays from pressure-swirl fuel injectors. PhD Thesis. Massachusetts Institute of
414 Technology (1999).
- 415 [5] VanDerWege, B. A., and Hochgreb S., Effects of fuel volatility and operating
416 conditions on fuel sprays in DISI engines:(1) Imaging investigation. No. 2000-01-0535.
417 SAE Technical Paper, (2000).
- 418 [6] VanDerWege, B. A., and Hochgreb , S.. Effects of fuel volatility and operating
419 conditions on fuel sprays in DISI engines:(2) PDPA investigation. No. 2000-01-0536.
420 SAE Technical Paper, (2000).
- 421 [7] Araneo, L., Coghe, A., Brunello, G. and Dondé, R., Effects of Fuel Temperature and
422 Ambient Pressure on a GDI Swirled Injector Spray, No. 2000-01-1901, SAE Technical
423 Paper Series, (2000).
- 424 [8] Dondé, R., Brunello, G., Araneo, L. and Coghe, A., Effect of Fuel Temperature on the
425 Mixing Properties of a GDI Spray, *Open Meeting on Combustion, 23rd Event of the*
426 *Italian Section of the Combustion Institute, V.2, (2000).*
- 427 [9] Araneo, L., Ben Slima, K. and Dondé, R., Flash boiling effect on swirled injector spray
428 angle, 18th Annual Conference on Liquid Atomization and Spray Systems ILASS-
429 Europe, (2002)
- 430 [10] Parrish S. E. and Zink R. J., Spray characteristics of multi-hole injectors under flash
431 boiling conditions, 21st Annual Conference on Liquid Atomization and Spray Systems
432 ILASS - Americas, (2008)
- 433 [11] Zhang, G., Xu, M., Zhang, Y., and Hung, D. L., Characteristics of flash boiling fuel
434 sprays from three types of injector for spark ignition direct injection (SIDI) engines. In
435 *Proceedings of the FISITA 2012 world automotive congress* (pp. 443-454). Springer
436 Berlin Heidelberg. (2013)
- 437 [12] Zeng, W., Xu, M., Zhang, G., Zhang, Y., and Cleary, D. J. Atomization and
438 vaporization for flash-boiling multi-hole sprays with alcohol fuels. *Fuel*, 95, 287-297
439 (2012).
- 440 [13] Yang, S., Song, Z., Wang, T., and Yao, Z.. An Experiment Study on Phenomenon and
441 Mechanism of Flash Boiling Spray from a Multi-hole Gasoline Direct Injector.
442 *Atomization and Sprays*, 23(5), 379-399, (2013).
- 443 [14] I Schmitz, A Leipertz, Comparison Of The Flash Boiling Influence On The Spray
444 Structure Of A High Pressure Swirl Injector And Of A Multihole Injector For Gdi
445 Engines - *10th International Conference on Liquid Atomization and Spray Systems*
446 Paper ID ICLASS06-026 (2006).

- 447 [15] Heldmann, M., Knorsch, T., Schmitz, I., Wensing, M., & Leipertz, A. Investigation of
448 significant spray rotation phenomena under flash-boiling conditions studied on a multi-
449 hole DISI injector for bio-ethanol E85 and gasoline E5. In 24th Annual Conference on
450 liquid atomization and spray systems ILASS - Europe), (2011)
- 451 [16] Weber, D., and Leick, P. Structure and Velocity Field of Individual Plumes of Flashing
452 Gasoline Direct Injection Sprays., 26th Annual Conference on Liquid Atomization and
453 Spray Systems, ILASS - Europe (2014)
- 454 [17] Mojtabi, M., Wigley, G., and Helie, J. The effect of flash boiling on the atomization
455 performance of gasoline direct injection multistream injectors. *Atomization and Sprays*,
456 24(6), 467-493.(2014)
- 457 [18] Mojtabi, M., Chadwick, N., Wigley, G. and Helie, J. The effect of flash boiling on
458 breakup and atomisation in GDI sprays. In Proceedings of the 22nd European
459 Conference on Liquid Atomization and Spray Systems. Paper ID ILASS08-6-1 (2008).
- 460 [19] Allocca, L., Montanaro, A., Di Gioia, R., and Bonandrini, G., Spray Characterization of
461 a Single-Hole Gasoline Injector under Flash Boiling Conditions No. 2014-32-0041. SAE
462 Technical Paper.(2014)
- 463 [20] Serras-Pereira, J., Van Romunde, Z., Aleiferis, P. G., Richardson, D., Wallace, S., &
464 Cracknell, R. F. Cavitation, primary break-up and flash boiling of gasoline, iso-octane
465 and n-pentane with a real-size optical direct-injection nozzle. *Fuel*, 89(9), 2592-2607.
466 (2010)
- 467 [21] Aleiferis, P. G., & Van Romunde, Z. R. An analysis of spray development with iso-
468 octane, n-pentane, gasoline, ethanol and n-butanol from a multi-hole injector under hot
469 fuel conditions. *Fuel*, 105, 143-168. (2013).
- 470 [22] Aleiferis PG, Serras-Pereira J, Augoye A, Davies TJ, Cracknell RF, Richardson D.
471 Effect of fuel temperature on in-nozzle cavitation and spray formation of liquid
472 hydrocarbons and alcohols from a real-size optical injector for direct injection spark-
473 ignition engines. *Int J Heat Mass Transfer* , 53, 4588–4606 (2010).
- 474 [23] Matsumoto, A., Xie, X., Zheng, Y., Lai, M. C., & Moore, W. Direct Injection Multi-hole
475 Spray and Mixing Characterization of Ethanol Gasoline Blends in Engine., 22nd Annual
476 Conference on Liquid Atomization and Spray System, ILASS Americas (2010)
- 477 [24] Postrioti, L., Bosi, M., Cavicchi, A., AbuZahra, F., Di Gioia, R., and Bonandrini, G.
478 Momentum Flux Measurement on Single-Hole GDI Injector under Flash-Boiling
479 Condition No. 2015-24-2480, SAE Technical Paper (2015).
- 480 [25] Moon, S., Bae, C., Abo-Serie, E. F., & Choi, J. Internal and near-nozzle flow of a
481 pressure-swirl atomizer under varied fuel temperature. *Atomization and Sprays*, 17(6),
482 529-550 (2007).
- 483 [26] Hung, D. L., Harrington, D. L., Gandhi, A. H., Markle, L. E., Parrish, S. E., Shakal, J. S.
484 and Kramer, J. L., Gasoline fuel injector spray measurement and characterization-a new
485 SAE J2715 recommended practice. *SAE International Journal of Fuels and Lubricants*,
486 1(2008-01-1068), 534-548 (2008).
- 487 [27] Settles, Gary S., Schlieren and shadowgraph techniques: visualizing phenomena in
488 transparent media. p. 42, Springer Science & Business Media, (2012).
- 489 [28] Lamanna, G., Kamoun, H., Weigand, B., & Steelant, J. Towards a unified treatment of
490 fully flashing sprays. *International Journal of Multiphase Flow*, 58, 168-184.(2014)
- 491 [29] Riazi M.R. , Characterization and properties of petroleum fractions, ASTM (2005)

- 492 [30] Olsen E., Method to calculate the vapour pressure of hydrocarbon solvents from simple
493 physic-chemical properties, National Institute of Occupational Health, Copenhagen
494 (2003) [http://www.esig.org/uploads/ModuleXtender/Publications/141/91-660-
vp_paper_olsen_june_2003-1-.pdf](http://www.esig.org/uploads/ModuleXtender/Publications/141/91-660-
495 vp_paper_olsen_june_2003-1-.pdf)
- 496 [31] Dutt N.V.K., “Estimation of Vapor Pressure from Normal Boiling Point of
497 Hydrocarbons”, Regional Research Laboratory, The Canadian Journal Of Chemical
498 Engineering. 60(5), 707–709 (1982)
- 499 [32] P.J. Linstrom and W.G. Mallard, Eds., NIST Chemistry WebBook, NIST Standard
500 Reference Database Number 69, National Institute of Standards and Technology,
501 Gaithersburg MD, 20899, <http://webbook.nist.gov>

Figure Captions

- Figure 1 Swirl injector near field spray semiangle variation with fuel temperature for different n-pentane/isooctane mixtures (a) and the same data plotted in terms of normalized pressure (saturation pressure/air pressure) [9]
- Figure 2 Spatial distribution of the injector jets at 30 mm distance from the tip.
- Figure 3 Image analysis steps for the near field angle measurement.
- Figure 4 Binary image of the near field spray in flash boiling conditions.
- Figure 5 Images of n-hexane spray in absence of flash boiling (a) and in flash boiling conditions (b)
- Figure 6 Near field (0-1mm) spray semiangles vs. fuel temperature at different chamber pressure: 0.1MPa (a), 0.08MPa(b), 0.06MPa (c), 0.04 MPa (d)
- Figure 7 Far field (20-30mm) spray semiangles vs. fuel temperature at different chamber pressure: 0.1MPa (a), 0.08MPa(b), 0.06MPa (c), 0.04 MPa (d)
- Figure 8 n-Hexane near field spray semiangle at different chamber air pressures in terms of injector tip temperature (a) and in terms of p_s/p_a (b)
- Figure 9 Near field spray semiangle of the tested pure hydrocarbons in terms of superheating degree ($T_f - T_s$)
- Figure 10 Near field spray semiangle of the tested pure hydrocarbons in terms of Jakob Number
- Figure 11 Near field spray semiangle of the tested pure hydrocarbons in terms of saturation pressure/air pressure ratio p_s/p_a
- Figure 12 Near and far field spray semiangles of all the tested pure hydrocarbons in terms of saturation pressure/air pressure ratio p_s/p_a
- Figure 13 Distillation curves of the tested gasolines
- Figure 14 Fuel 04 ASTM-D86 and calculated True Boiling Point curves
- Figure 15 Saturation pressure curves of the tested fuels (temperature in reciprocal scale)
- Figure 16 Near and far field spray semiangle of all the tested fuels in terms of saturation pressure/air pressure ratio p_s/p_a
- Figure 17 Fuel95 near field spray semiangle at different chamber air pressures in terms of fuel temperature
- Figure 18 Saturation pressure curve of Fuel95 calculated from spray semiangle at different chamber pressure

Fuels	n-hexane, n-heptane, isooctane, Fuel04, Fuel06, Fuel 08, Fuel95
Injection pressure	10 MPa
Chamber pressure	40kPa, 60kPa, 80kPa, atmospheric
Injector temperature	30, 50, 70, 90, 110 °C

Table 1 - Experimental conditions

Figure 1

[Click here to download high resolution image](#)

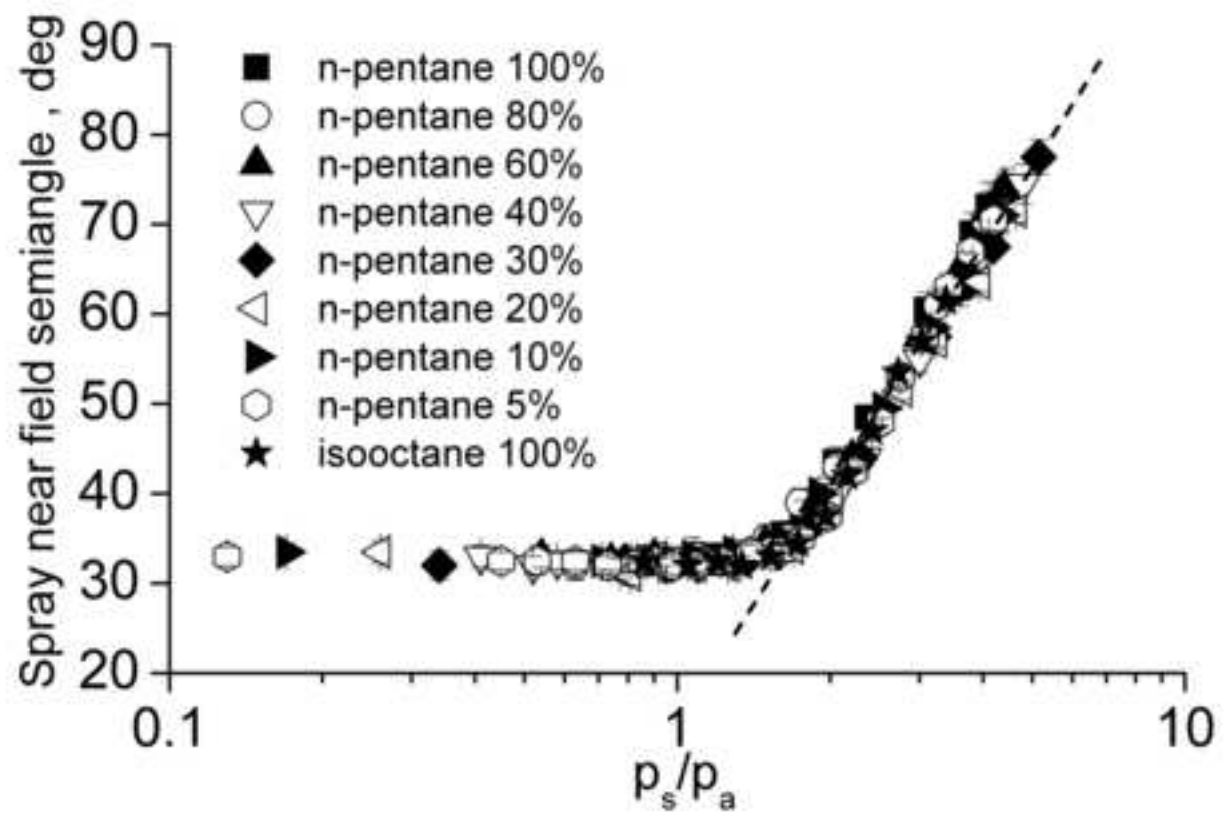
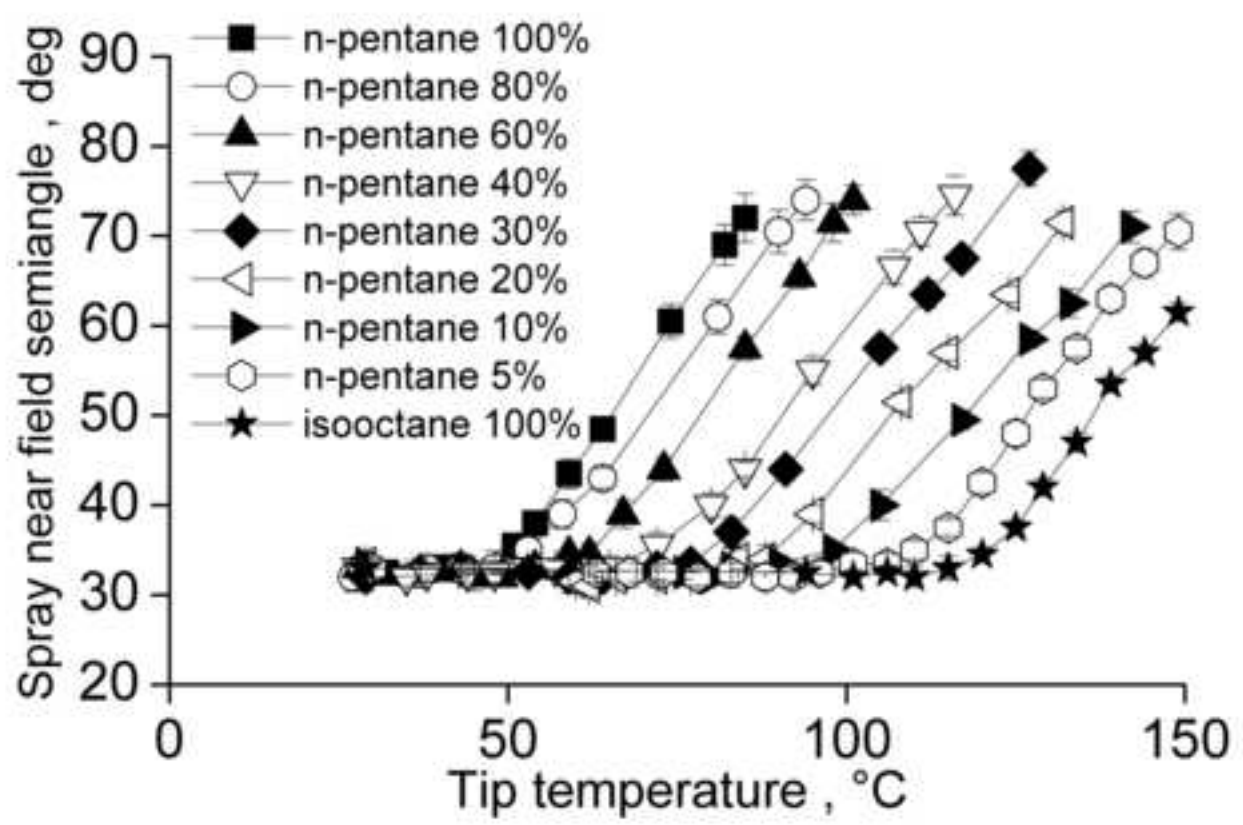


Figure 2
[Click here to download high resolution image](#)

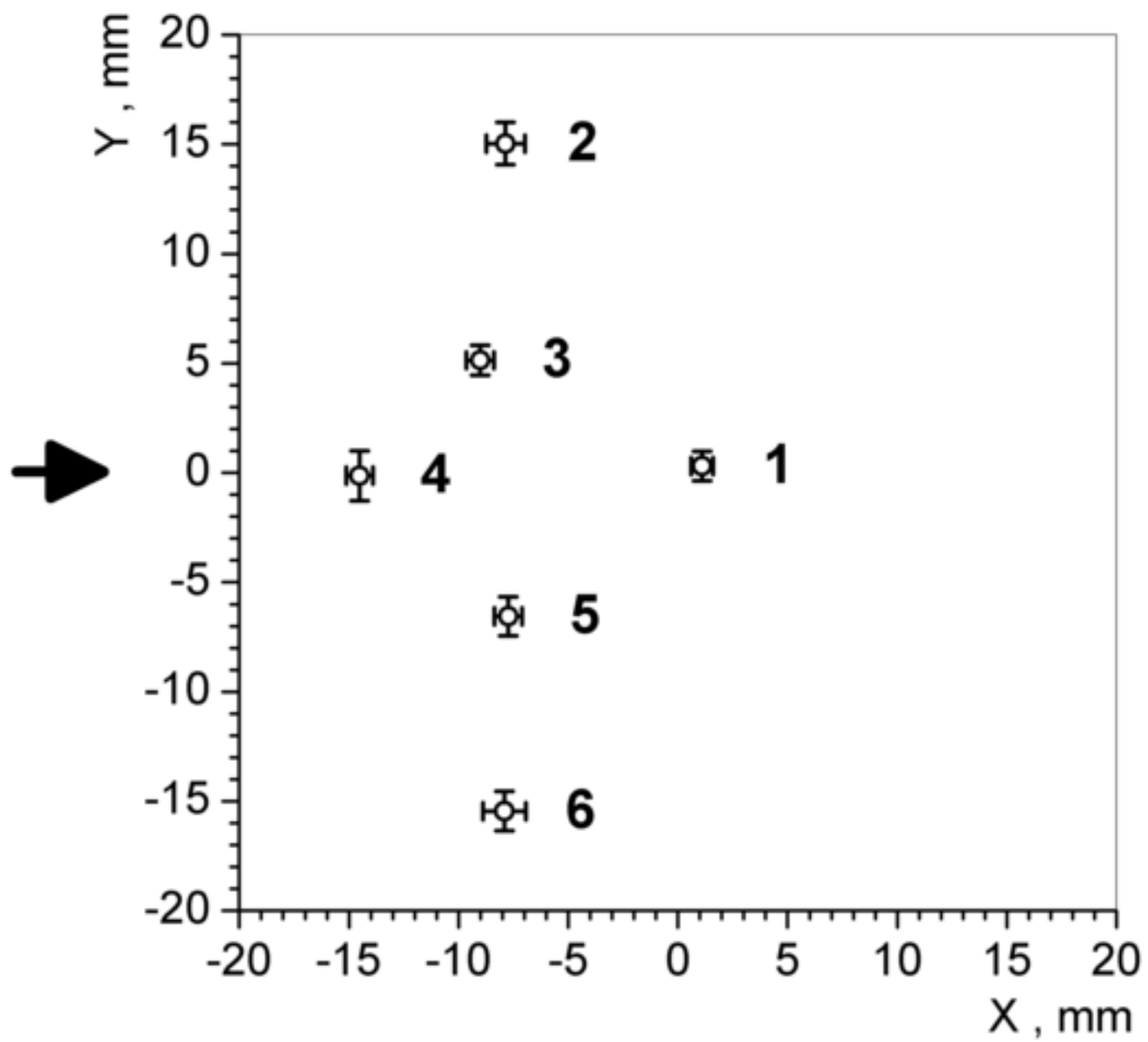


Figure 3
[Click here to download high resolution image](#)

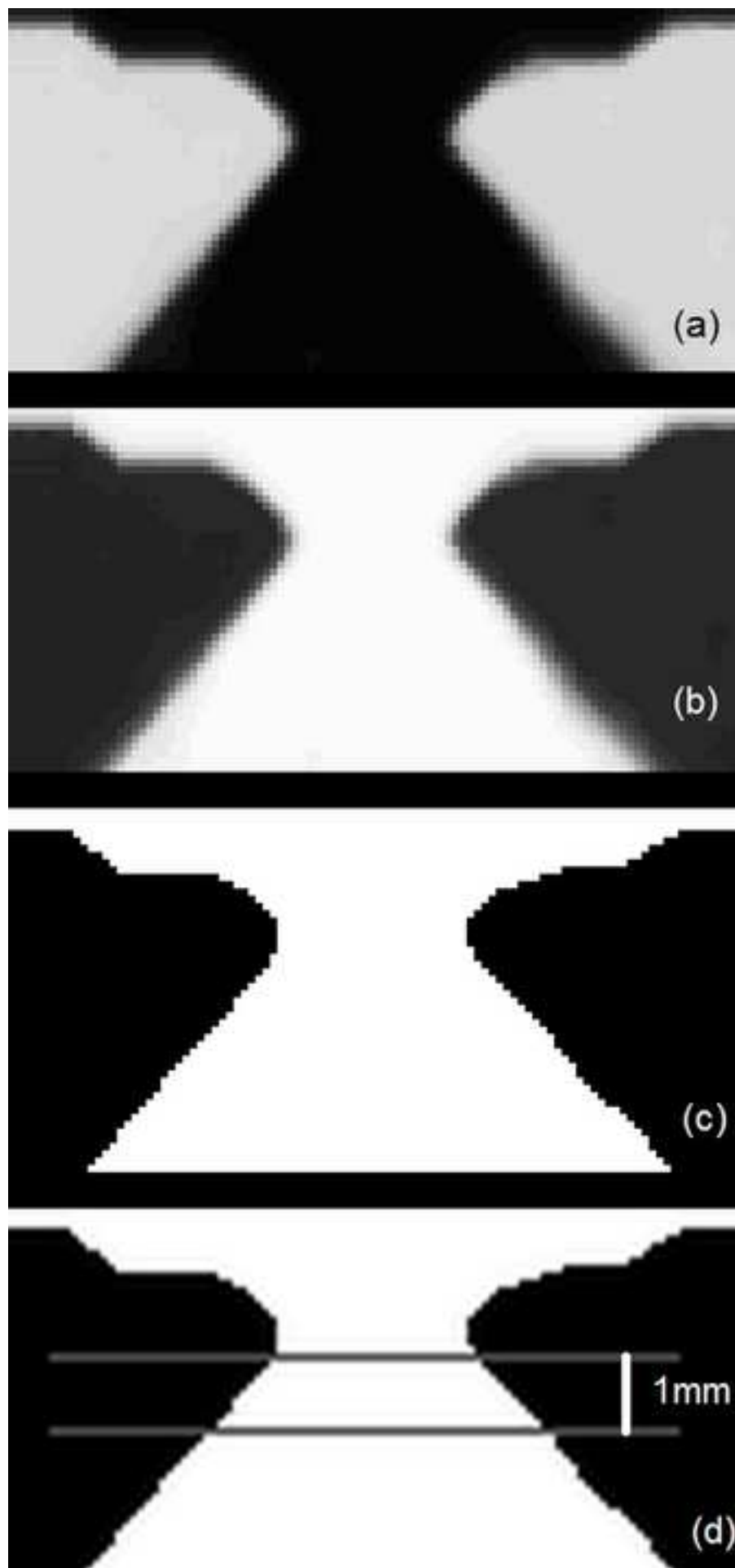


Figure 4
[Click here to download high resolution image](#)



Figure 5
[Click here to download high resolution image](#)

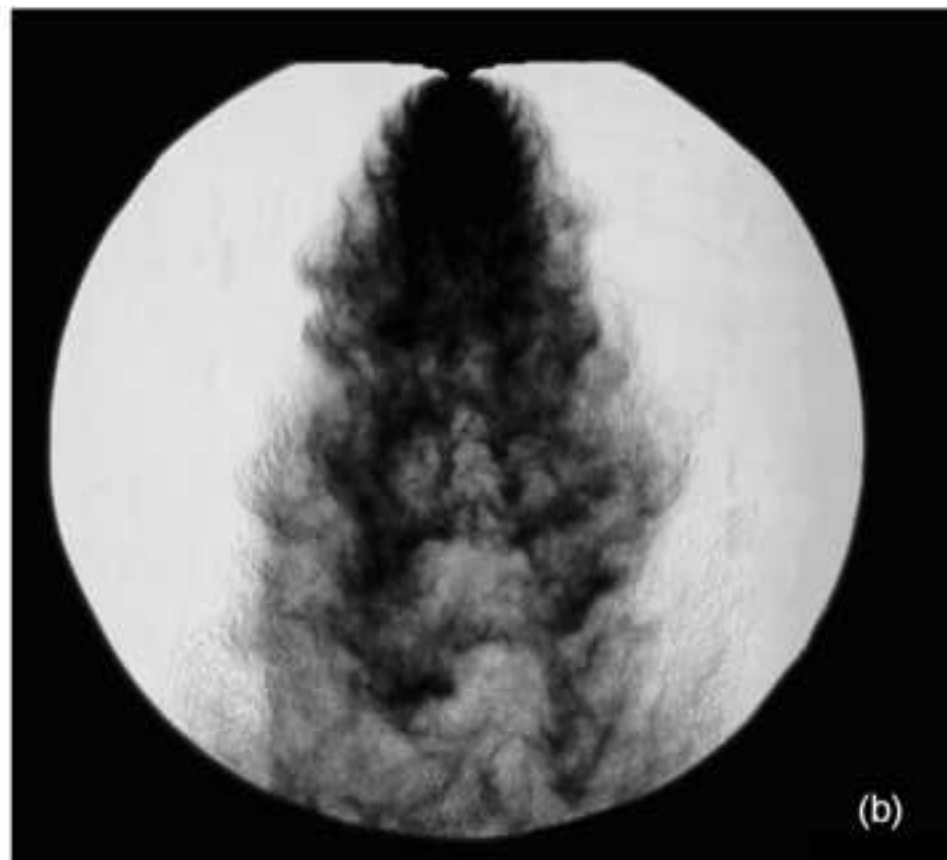
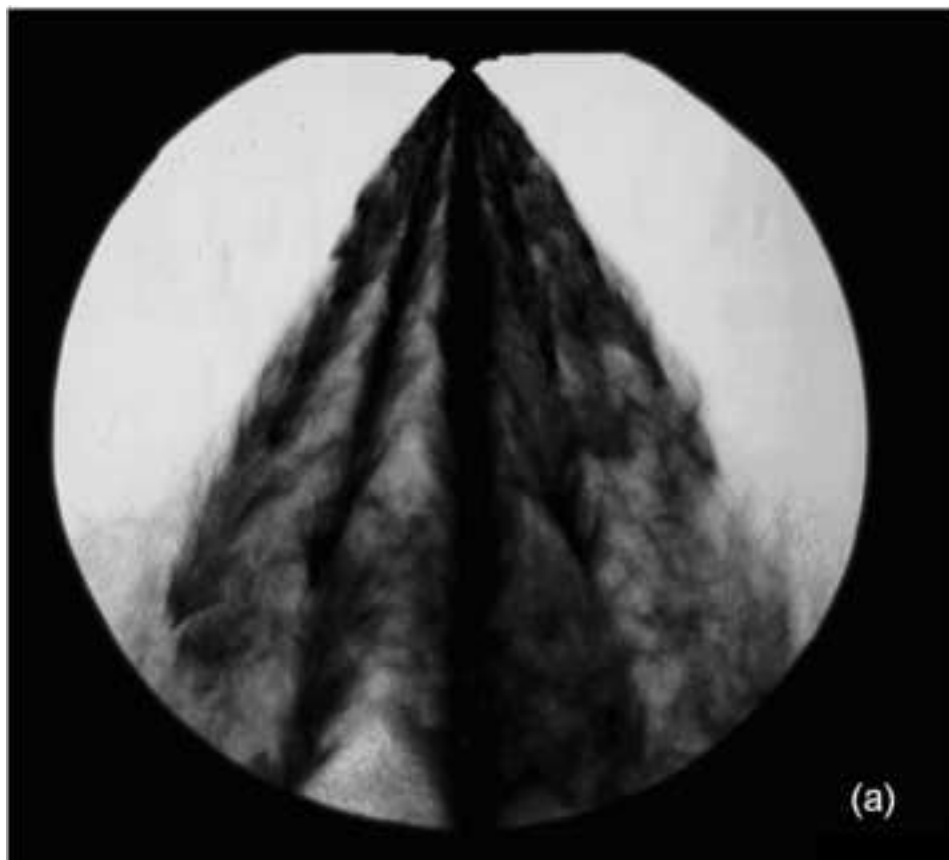


Figure 6
[Click here to download high resolution image](#)

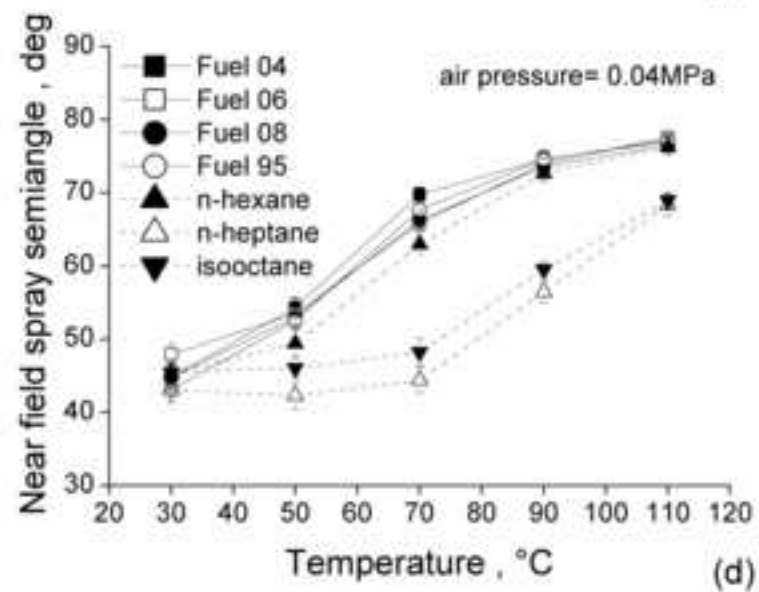
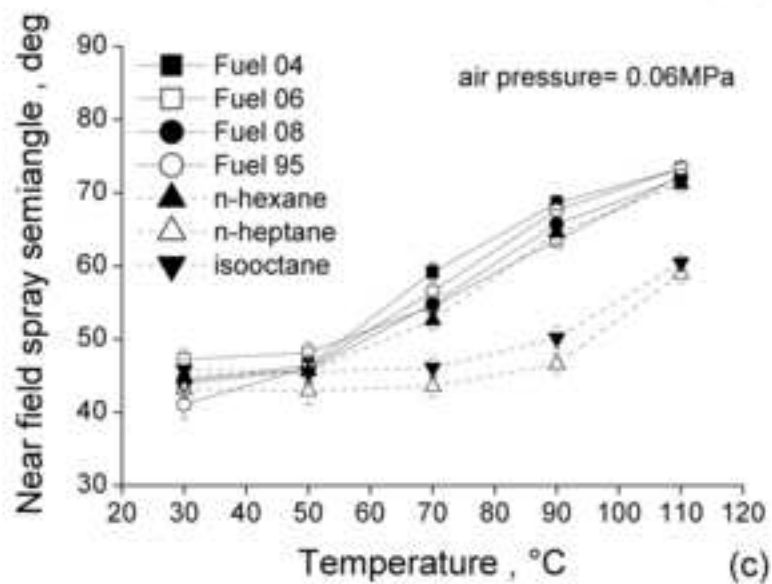
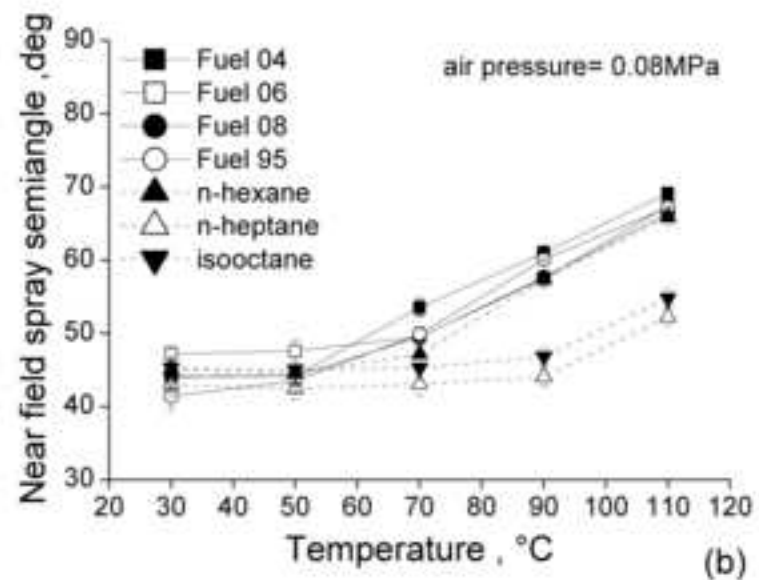
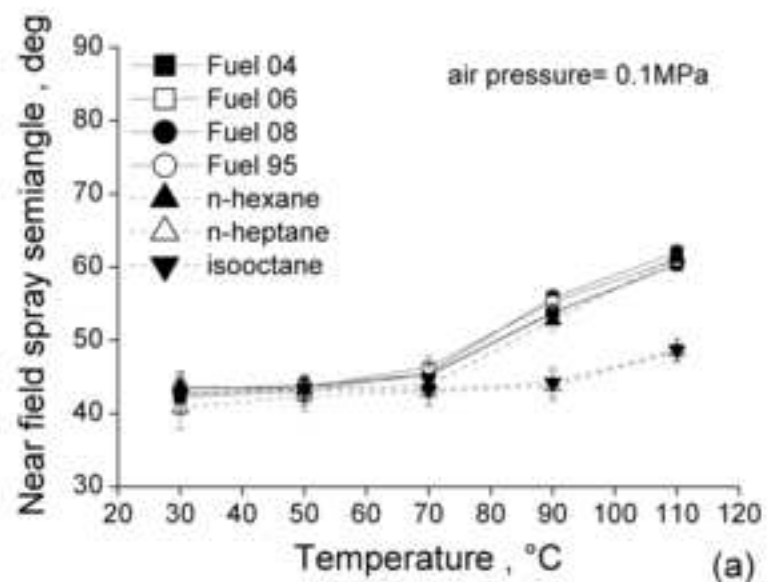


Figure 7
[Click here to download high resolution image](#)

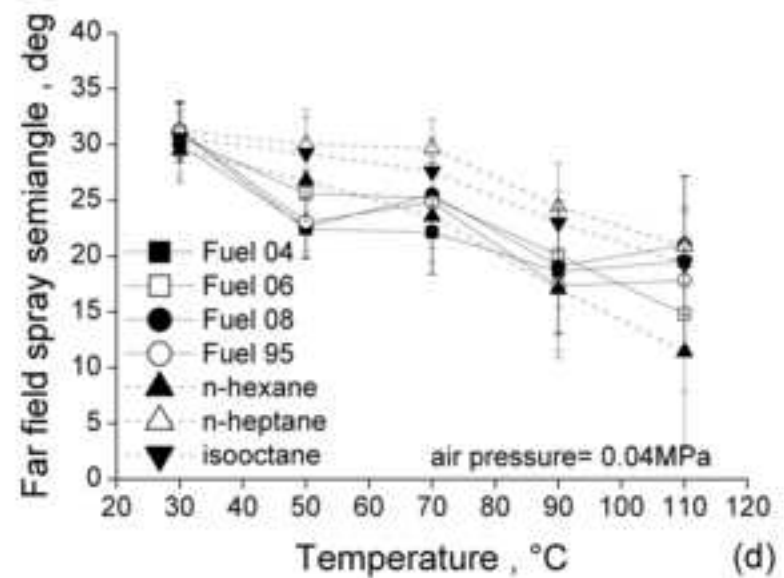
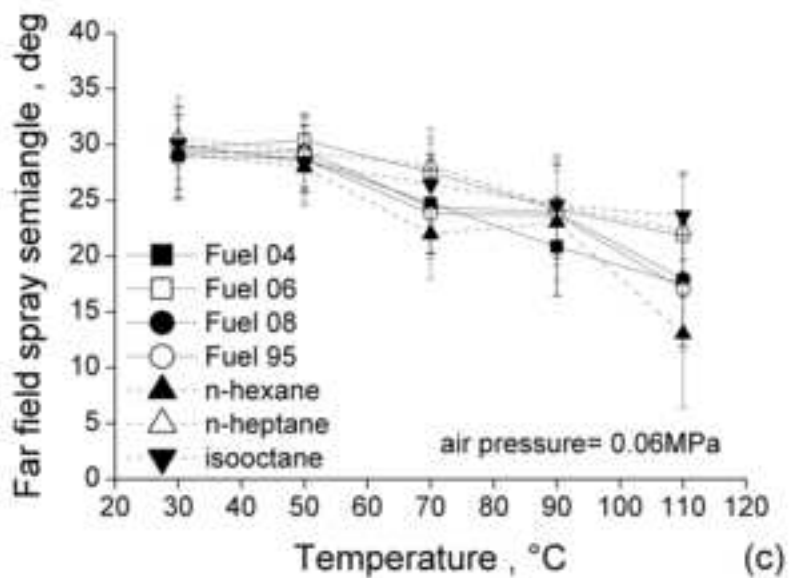
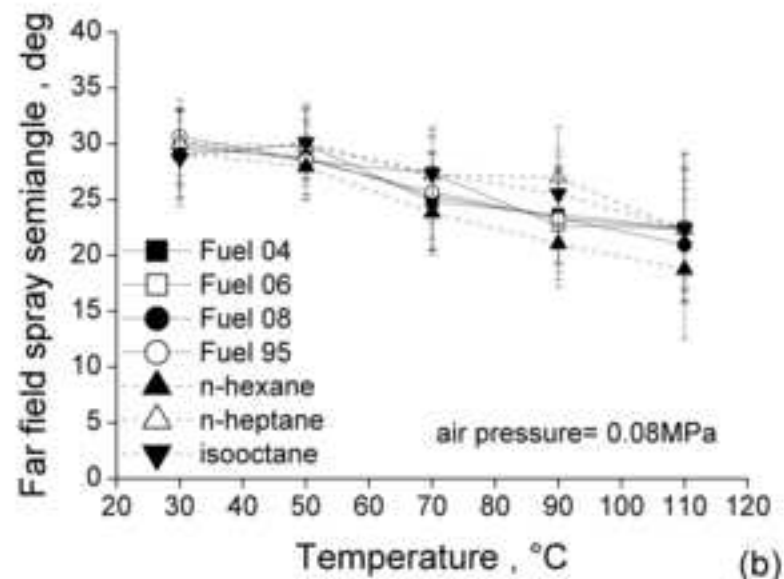
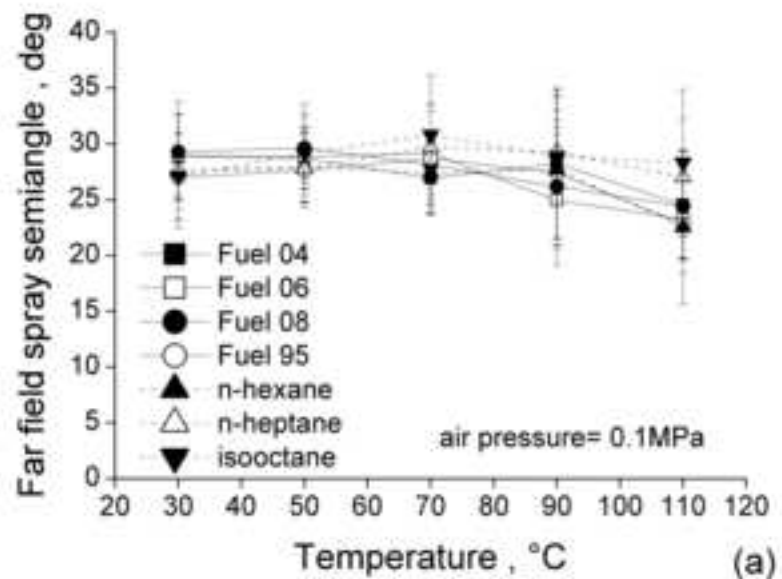


Figure 8
[Click here to download high resolution image](#)

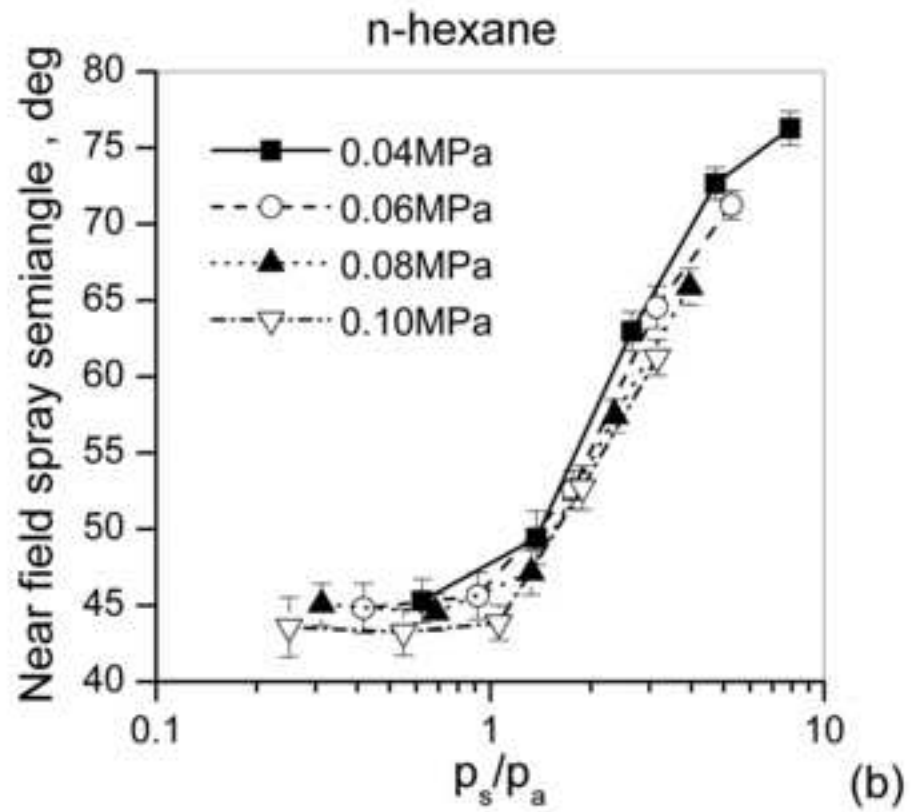
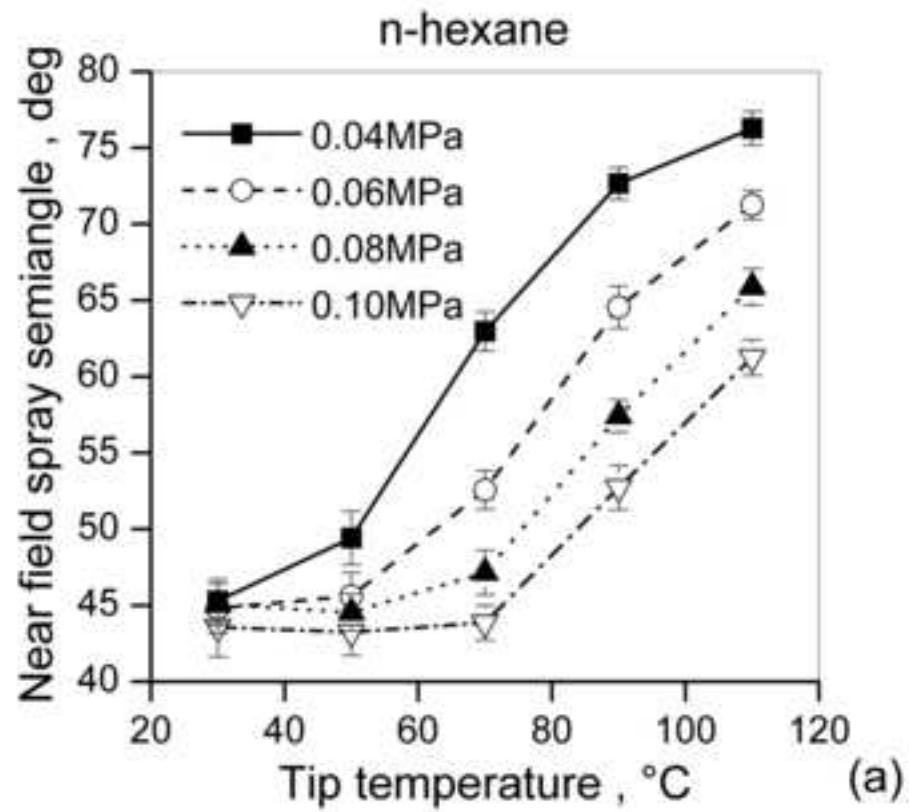


Figure 9
[Click here to download high resolution image](#)

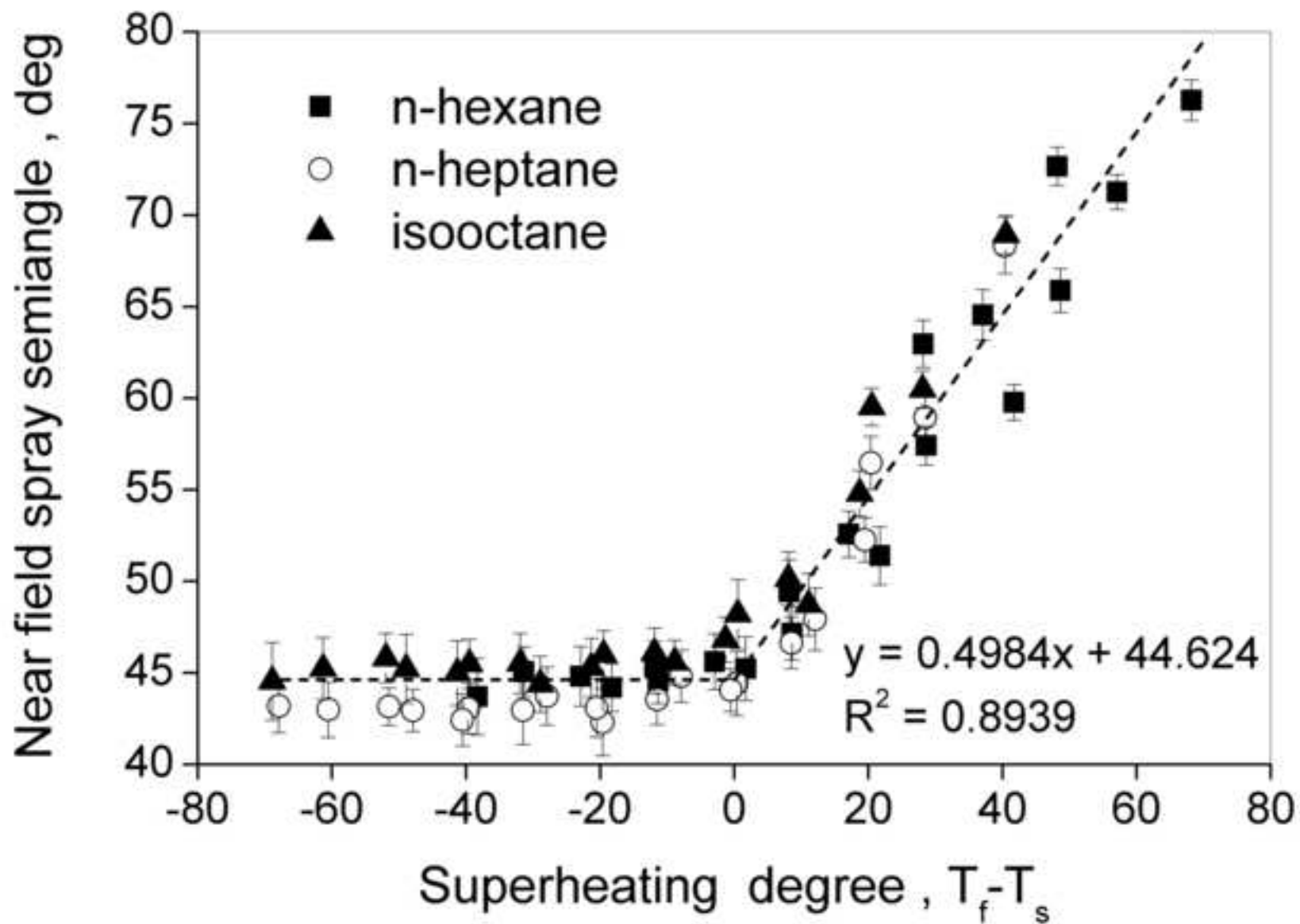


Figure 10

[Click here to download high resolution image](#)

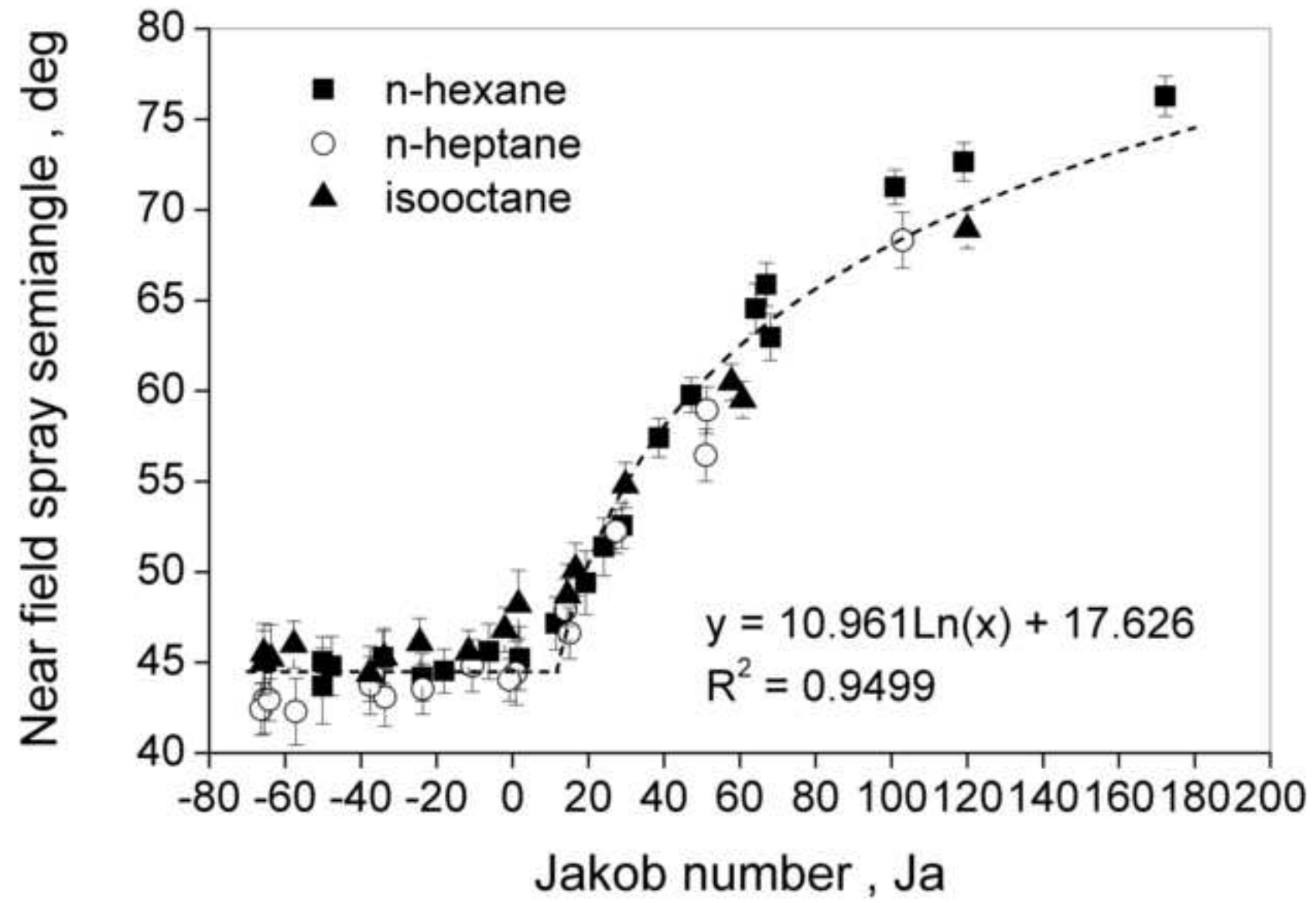


Figure 11
[Click here to download high resolution image](#)

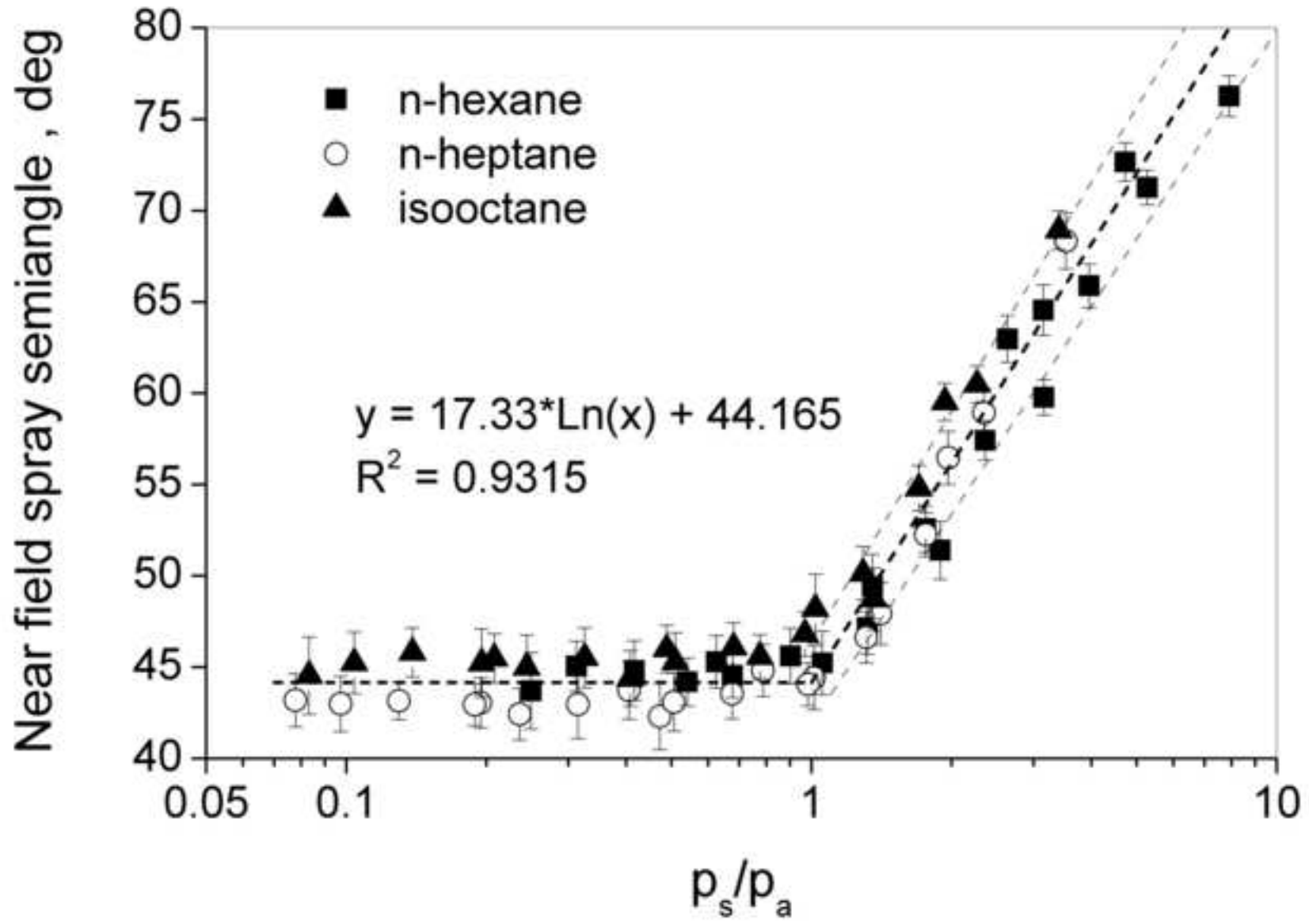


Figure 12

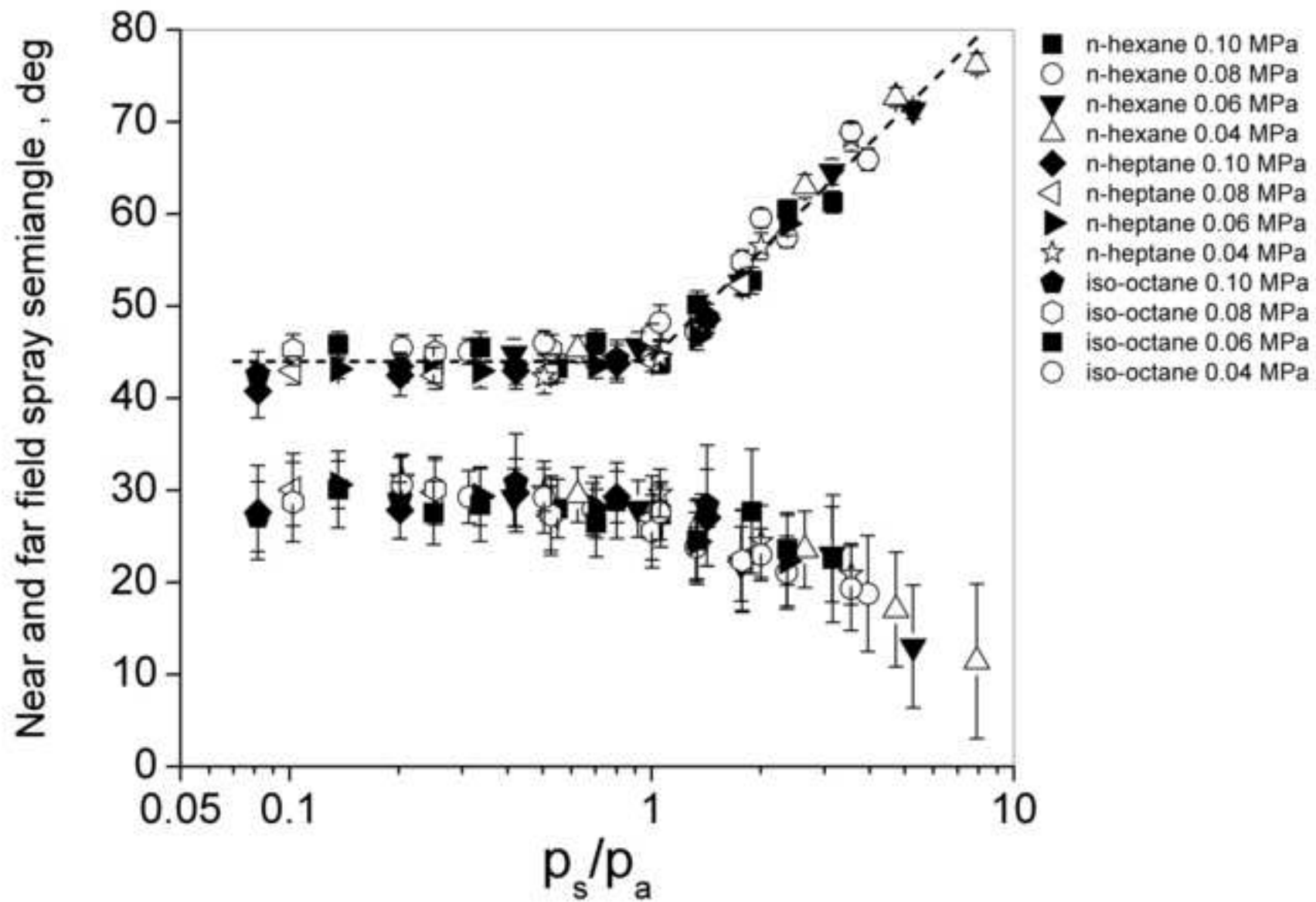
[Click here to download high resolution image](#)

Figure 13
[Click here to download high resolution image](#)

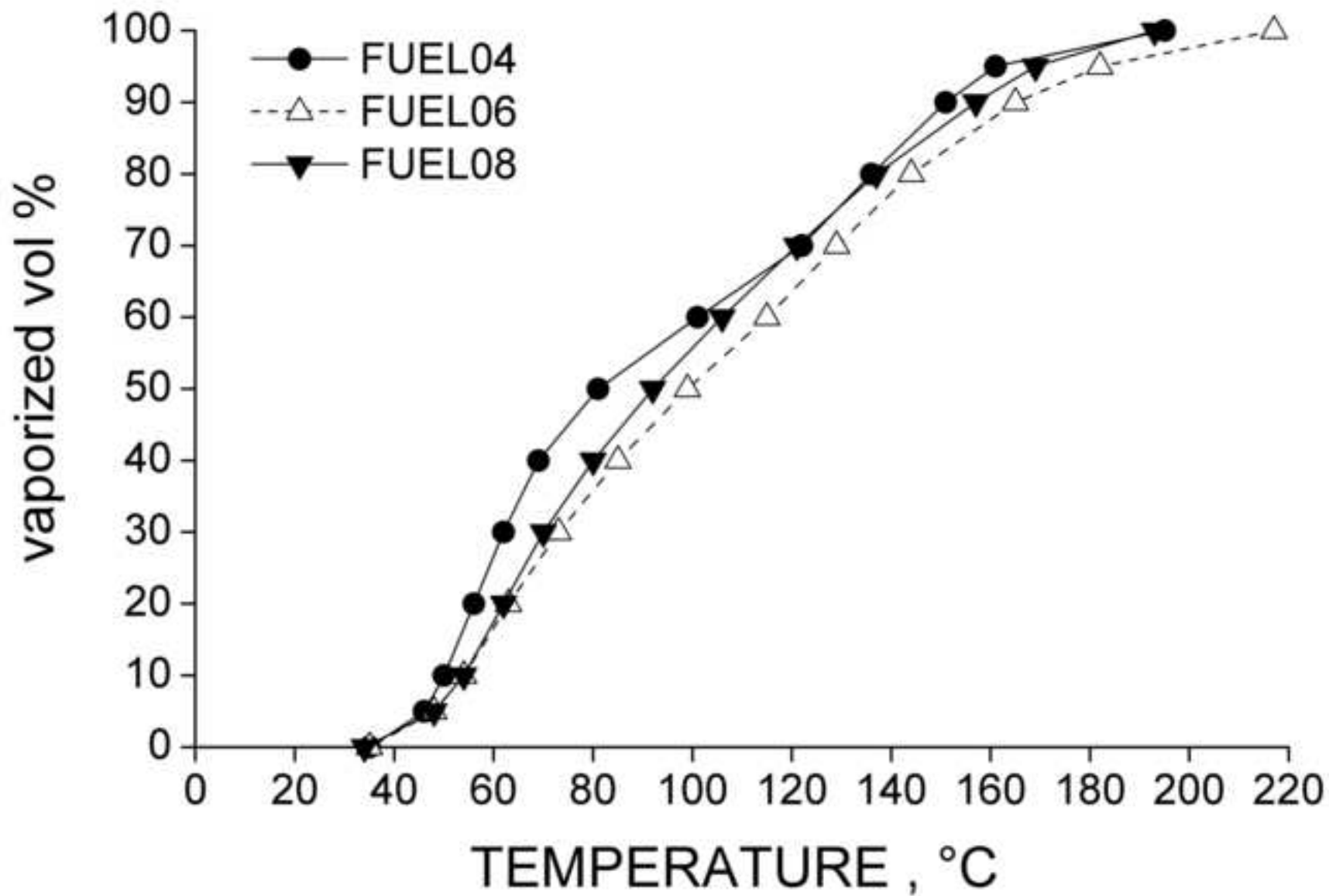


Figure 14
[Click here to download high resolution image](#)

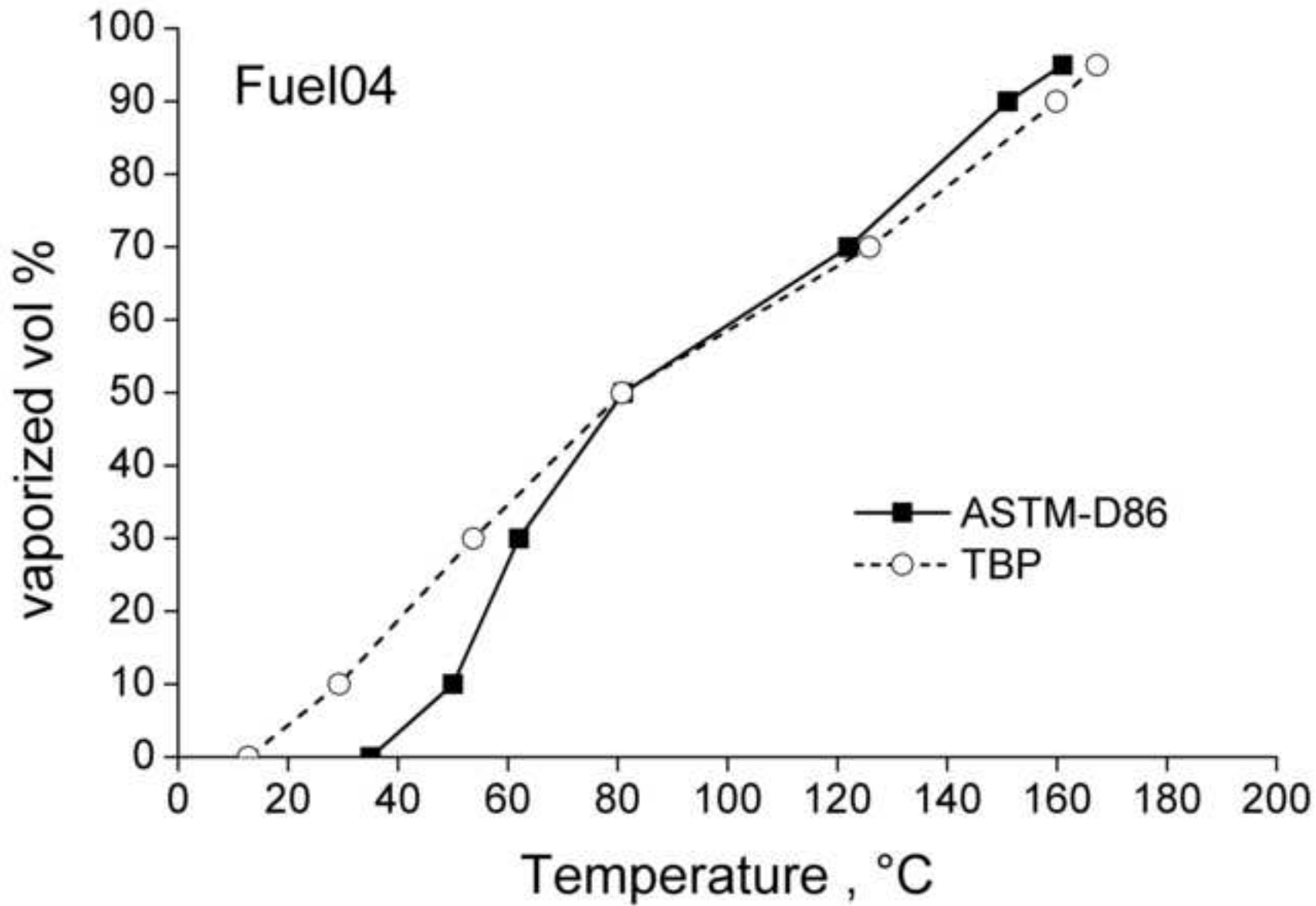


Figure 15

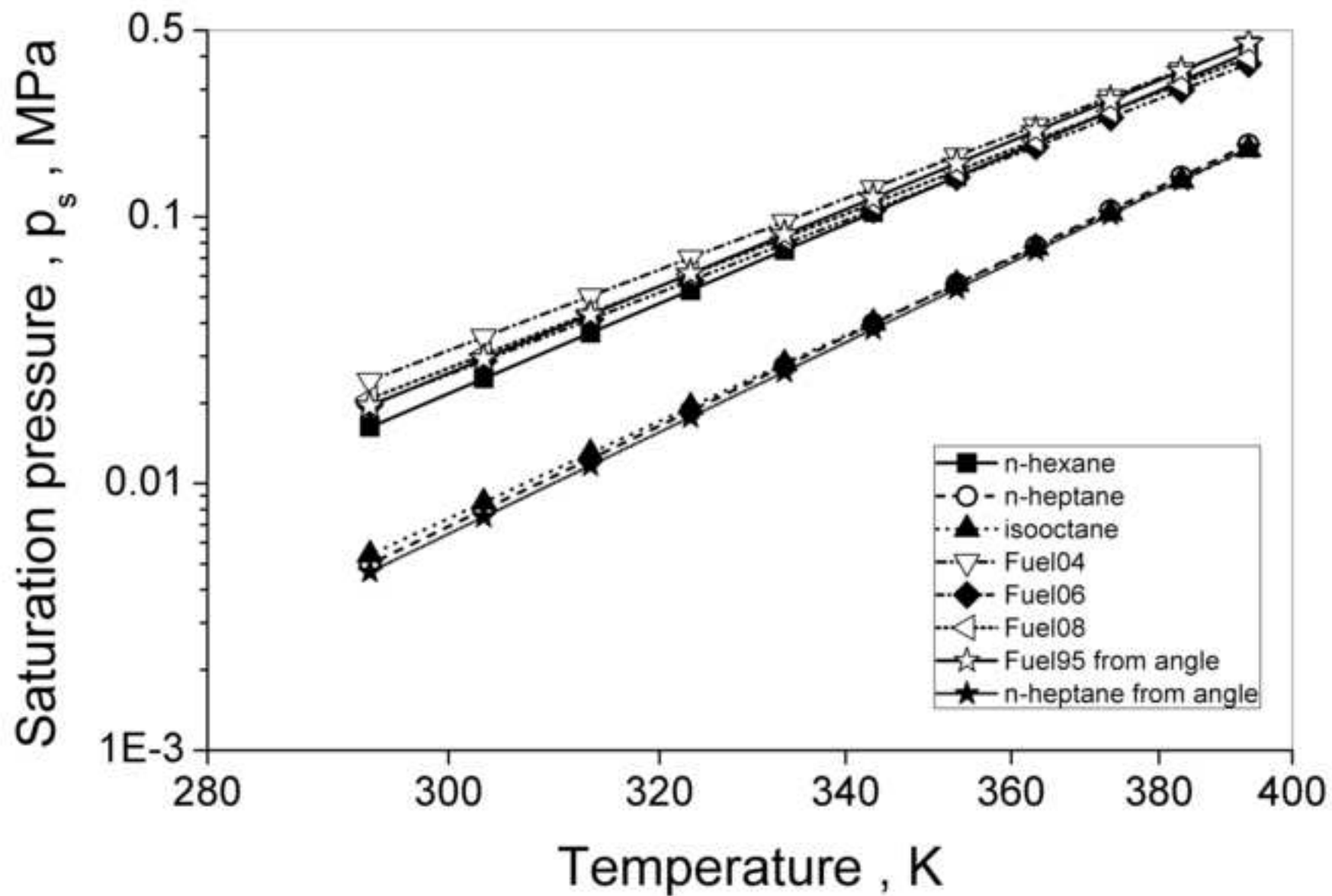
[Click here to download high resolution image](#)

Figure 16

[Click here to download high resolution image](#)

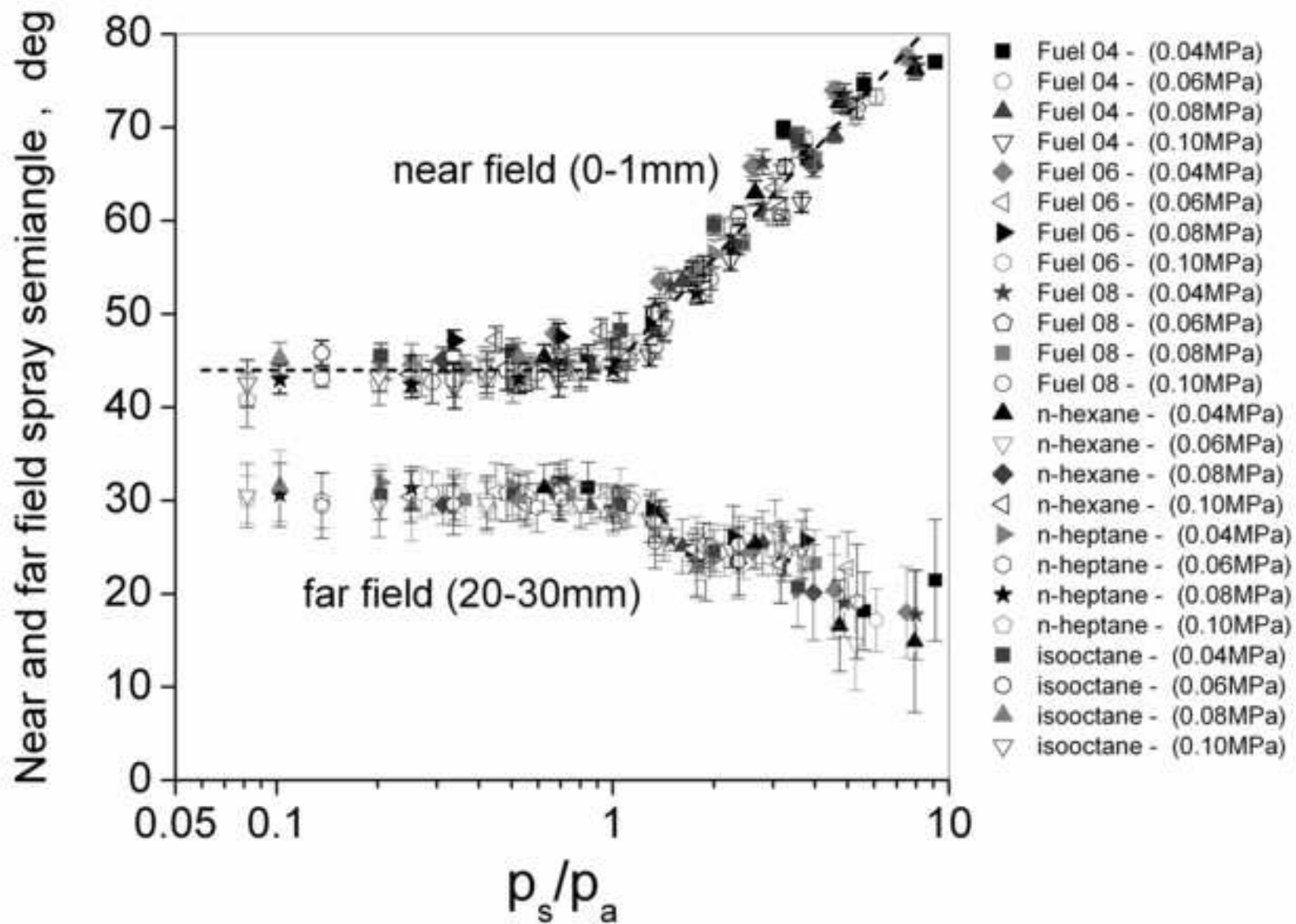


Figure 17

[Click here to download high resolution image](#)

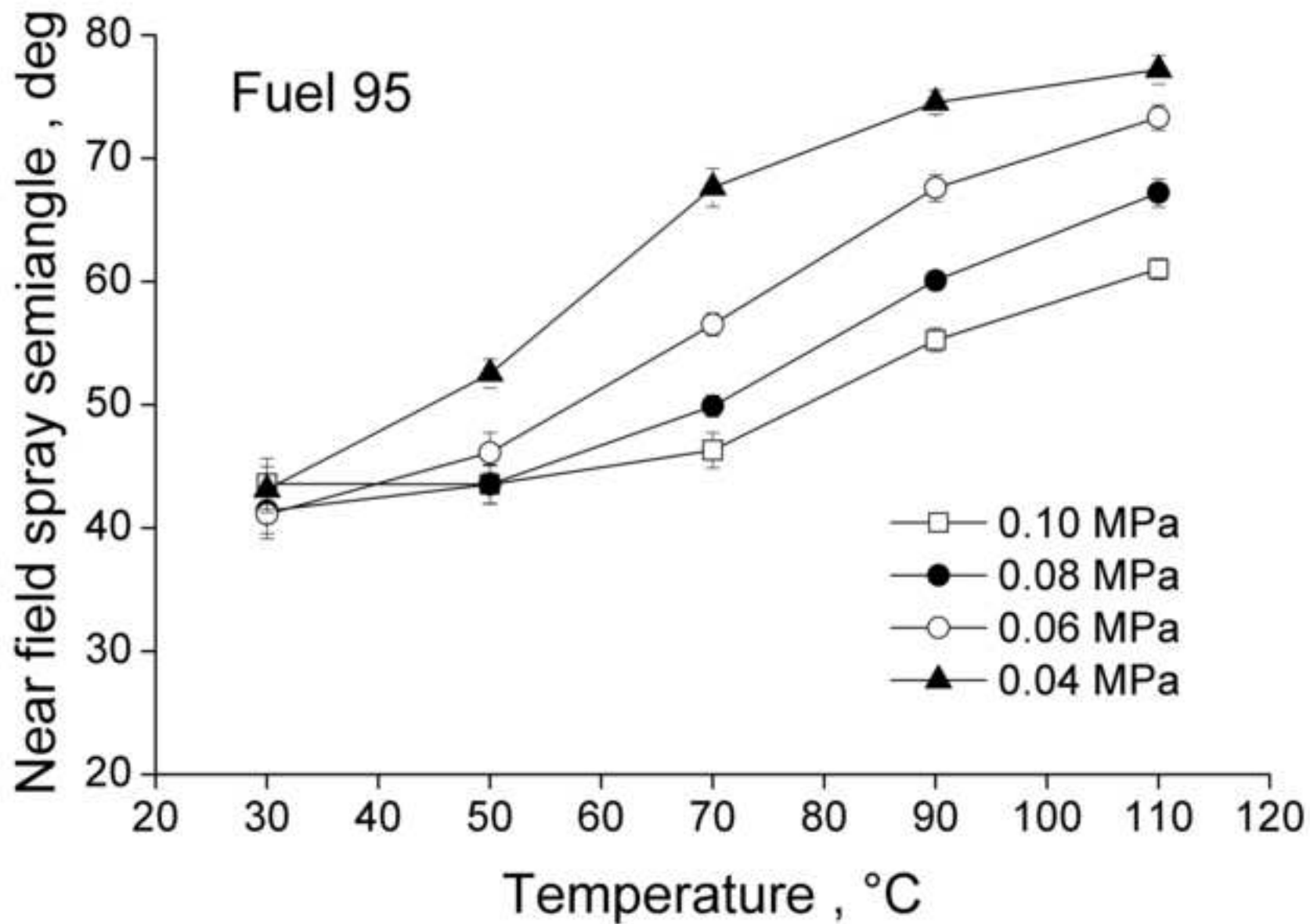


Figure 18

[Click here to download high resolution image](#)

